# MODELING OF GROUND-BORNE VIBRATION FROM UNDERGROUND RAILWAY SYSTEMS

A THESIS SUBMITTED TO
THE GRADUATE SCHOOL OF NATURAL AND APPLIED SCIENCES
OF
MIDDLE EAST TECHNICAL UNIVERSITY

BY

AHMET ALBAYRAK

IN PARTIAL FULFILLMENT OF THE REQUIREMENTS
FOR
THE DEGREE OF MASTER OF SCIENCE
IN
MECHANICAL ENGINEERING

NOVEMBER 2012

Approval of the thesis:

**MODELING OF GROUND-BORNE VIBRATION FROM UNDERGROUND RAILWAY SYSTEMS**

submitted by **AHMET ALBAYRAK** in partial fulfillment of the requirements for the degree of **Master of Science in Mechanical Engineering Department, Middle East Technical University** by,

Prof. Dr. Canan Özgen _____
Dean, Graduate School of **Natural and Applied Sciences**

Prof. Dr. Suha Oral _____
Head of Department, **Mechanical Engineering**

Prof. Dr. Mehmet Çalışkan _____
Supervisor, **Mechanical Engineering Dept., METU**

**Examining Committee Members:**

Prof. Dr. Y. Samim Ünlüsoy _____
Mechanical Engineering Dept., METU

Prof. Dr. Mehmet Çalışkan _____
Mechanical Engineering Dept., METU

Asst. Prof. Dr. Ergin Tönük _____
Mechanical Engineering Dept., METU

Asst. Prof. Dr. Yiğit Yazıcıoğlu _____
Mechanical Engineering Dept., METU

Assoc. Prof. Dr. Ahmet Türer _____
Civil Engineering Dept., METU

Date _____

**I hereby declare that all information in this document has been obtained and presented in accordance with academic rules and ethical conduct. I also declare that, as required by these rules and conduct, I have fully cited and referenced all material and results that are not original to this work.**

Name, Last name : Ahmet Albayrak

Signature :

## ABSTRACT

MODELING OF GROUND-BORNE VIBRATION FROM UNDERGROUND RAILWAY SYSTEMS

Albayrak, Ahmet
M.S, Department of Mechanical Engineering
Supervisor: Prof. Dr. Mehmet Çalışkan

November 2012, 86 pages

Ground-borne vibrations from railway systems not only pose threats to structural integrity of nearby buildings and cause annoyance on people but also contribute into environmental noise levels. It is of utmost importance to predict these vibrations at the design stage of such systems. This thesis attempts to reach this goal through finite elements analysis. Commercial software is used to develop a finite element model of an existing railway system. The model is based on the work of Forrest and Hunt [11]. It is also aimed to perform transient analysis in time domain to complement vibration information already obtained in frequency domain. The model is validated by checking maximum element size and comparing results with the infinite boundary condition case. Parametric studies are designed to investigate effects of soil type, railpad type and train speed on vibrations induced by underground train traffic. Results acquired through the finite element analysis are found to be in good harmony with the ones by existing numerical methods. The study demonstrates that the approach can be applied to predict ground-borne vibration from any configuration of railway systems.

**Keywords**: Ground-borne vibration, finite element modeling, railway vibration

# ÖZ

YERALTI DEMİRYOLU SİSTEMLERİNDEN KAYNAKLANAN TİTREŞİMİN MODELLENMESİ

Albayrak, Ahmet
Yüksek Lisans, Makina Mühendisliği Bölümü
Tez Yöneticisi: Prof. Dr. Mehmet Çalışkan

Kasım 2012, 86 sayfa

Toprak yoluyla taşınan titreşim sadece yakındaki binaların yapısını tehdit edip insanlara rahatsızlık vermekle kalmaz aynı zamanda çevresel gürültüye de katkı sağlar. Bu titreşimlerin tasarım aşamasında öngörülebilmesi oldukça önemlidir. Bu tezde sonlu elemanlar analiziyle bu amaca ulaşmak amaçlanmıştır. Ticari bir yazılım kullanılarak yeni işletmeye açılan bir yeraltı metro sisteminin sonlu eleman modeli geliştirilmiştir. Geliştirilen model Forrest ve Hunt [11]'ın modeline dayanmaktadır. Bu tezde frekans aralığında elde edilen titreşim bilgisine tamamlayıcı olarak zamana bağlı analiz de gerçekleştirilmiştir. Modelin geçerliliği en büyük eleman boyutunun kontrol edilmesiyle ve sonuçların sonsuz sınır koşul sonuçlarıyla karşılaştırılmasıyla sağlanmıştır. Toprak çeşidi, ray altı pedi çeşidi ve tren hızının etkisinin araştırılması için parametrik çalışmalar yapılmıştır. Sonlu eleman analizinden elde edilen sonuçlar, sayısal yöntemlerle hesaplananlar ile uyum göstermektedir. Bu yaklaşımın herhangi bir demiryolu sisteminin toprak yoluyla taşınan titreşiminin öngörüsünde kullanılabileceği gösterilmiştir.

**Anahtar kelimeler**: toprak yoluyla taşınan titreşim, sonlu elemanlar modellemesi, demir yolu titreşimi

*To my family…*

**ACKNOWLEDGEMENTS**

I would like to thank my supervisor, Prof. Dr. Mehmet Çalışkan, for his continuous support, motivation and guidance from beginning to end of this thesis.

I am grateful for the support of Mr. Salih Alan during every step of the thesis.

I also owe many thanks to Mr. İsmet Baran for technical assistance and guidance throughout the thesis.

Finally, I would like to thank my parents Perihan and İrfan Albayrak, for unconditional love, support and encouragement.

## TABLE OF CONTENTS

## LIST OF FIGURES

FIGURES

## LIST OF TABLES

TABLES

## LIST OF SYMBOLS

SYMBOLS

EI, bending stiffness

A, cross sectional area

q(x, t), load on the beam

t, time

G, shear modulus

k, shear factor

$k_r$, stiffness of railpad

$c_r$, viscous damping of railpad

$Y_{w1}$, Lateral motion DOF

$Z_{w1}$, Vertical motion DOF

$\phi_{w1}$, Roll motion DOF

$\beta_{w1}$, Pitch motion DOF

$\psi_{w1}$, Yaw motion DOF

$L_d$, $\lambda$, wavelength of irregularity

$Z_W(\omega)$, wheel impedance

$Z_R(\omega)$, rail impedence

$S_X(\omega)$, power spectral density function

$A_v$, line grade coefficient

$\omega_c$, line grade coefficient

a, unevenness parameter

b, waviness parameter

f, frequency

$C_H$, Hertzian constant

$k_w$, dynamic stiffness of wheel

$k_s$, dynamic stiffness of bogie

$k_c$, dynamic stiffness of car

$\alpha$, viscous damping component

$\beta$, hysteresis damping component

$\xi$, damping ratio

$\eta$, loss factor

$\delta$, excitation due to irregularity

$\Delta$, amplitude of excitation due to irregularity

u, displacement components in x direction

v, displacement components in y direction

w, displacement components in z direction

$\omega$, angular frequency

$\zeta$, angular wavenumber

n, number of waves developed around the circumference

a, radius of the shell

h, thickness of the shell

E, Young's modulus

$\nu$, Poisson's ratio

$\varrho$, density of the medium

m, beam's mass per unit length

L, axle spacing

v, vehicle speed

N, number of axle masses

$m_c$, mass of 1/8 vagon

$m_b$, mass of bogie

$m_w$, mass of wheelset

$k_1$, primary vertical stiffness

$k_2$, secondary vertical stiffness

$c_1$, primary vertical damping

$c_2$, secondary vertical damping

# CHAPTER 1

## INTRODUCTION

Technological and industrial developments have serious adverse effects on environment. One of the greatest problems that the world is facing today is environmental pollution, increasing with every passing year and causing grave and irreparable damage to the earth. Environmental pollution consists of five basic types of pollution, namely, air, water, soil, noise and light. Noise pollution is damaging the environment at an alarming rate. It also affects human health and behavior. Poor urban planning may give rise to noise pollution, since side-by-side industrial and residential buildings can result in noise pollution in the residential area.

The source of most outdoor noise worldwide is mainly due to transportation systems. Especially, railway transportation plays a big role in noise pollution because of the ground-borne vibrations from railway systems. Legislative regulations are enforced to control the noise level in cities and comprehensive studies are conducted to decrease the noise levels. Besides noise, vibrations originating from railway systems also cause annoyance and hazards to the people and buildings nearby. Several standards are serviced to limit such vibrations. An ISO standard, ISO 2631 is devoted to provide guidelines and criteria. Particularly, ISO 2631-2:1989 or TS ISO 2631-2, which is evaluation of human exposure to whole-body

vibration -- Part 2: Continuous and shock-induced vibrations in buildings (1 to 80 Hz) which outlines measures and vibration criteria to be enforced for vibration mitigation.

## 1.1 GROUND-BORNE VIBRATION

As cities grow, the demand for transportation also increases and railway transportation offers a good solution to the transportation problem. It both saves space and time. However, a big problem comes together with this type of transportation. Vibrations generated by train movements propagate through the tunnel and surrounding soil, into the structure of the buildings nearby. After this ground borne vibration reaches to the building, it is radiated as noise. (Figure 1.1)

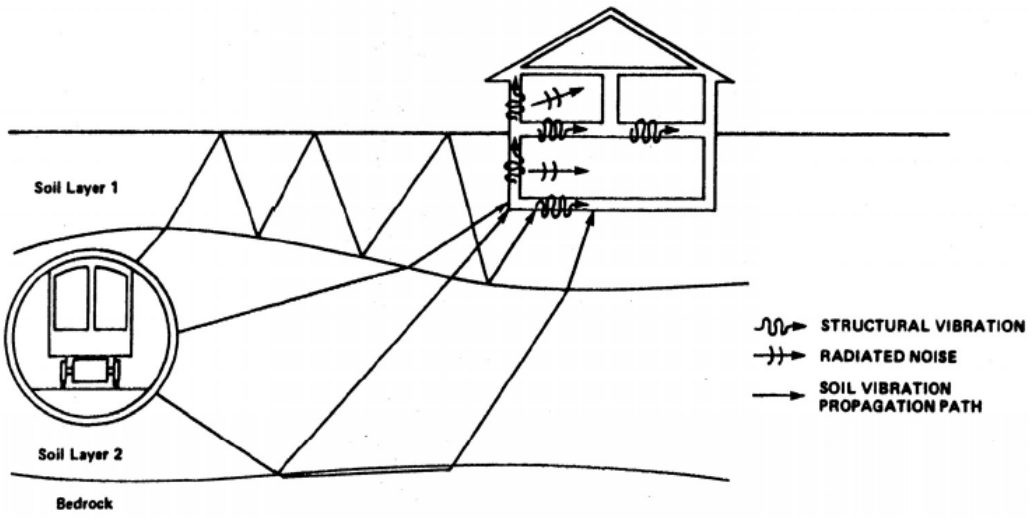


Figure 1.1 Propagation paths of the vibration induced by train [9]

Eitzenberger [9] classified propagation stages of these vibrations into three groups as source, path and receiver. The propagation process is explained in every step how train induced vibration is radiated as noise to the occupants of dwellings. (Figure 1.2)

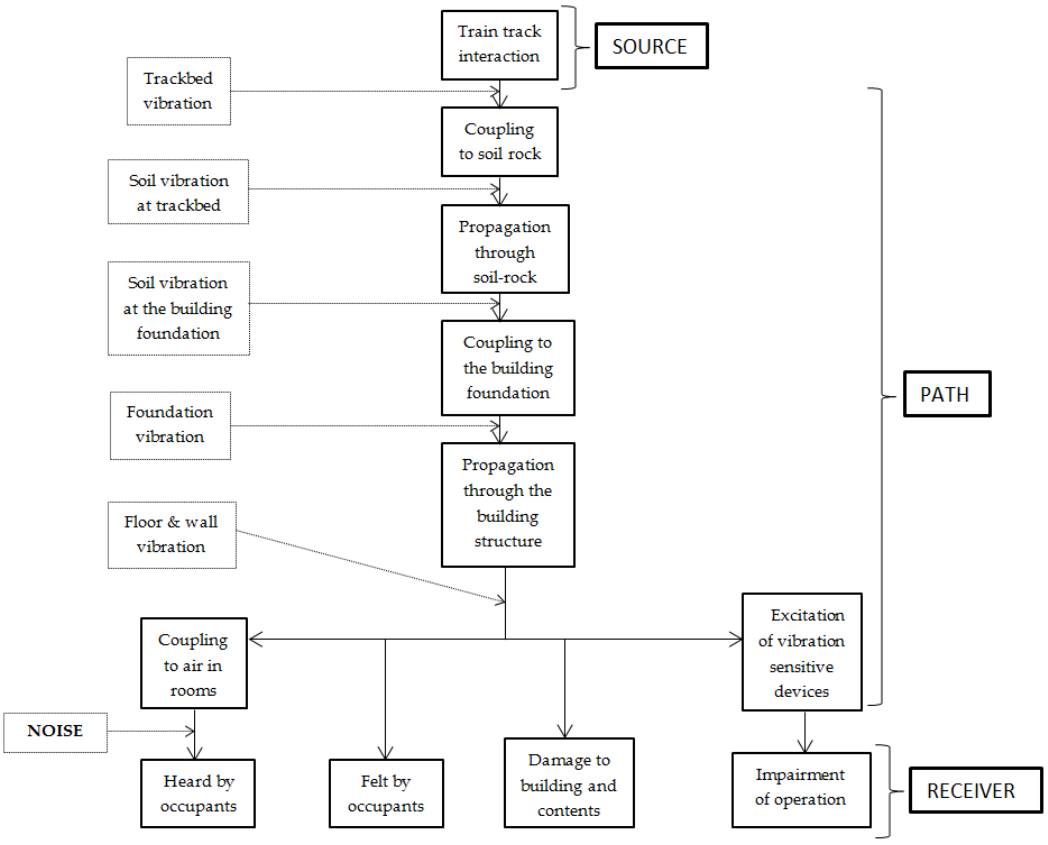


Figure 1.2 Block diagram illustrating the different stages of vibration propagation [9]

In order to decrease the noise, different methods and techniques can be used with respect to the vibration source. Vibration source, therefore, should be identified in detail to provide a feasible and working solution.

## 1.2 VIBRATION SOURCES

There are many parameters and excitation types which influence the level and characteristics of train-induced vibrations, as outlined in Table 1.1.

Table 1.1 Sources of vibration [9,12,13]

| | |
|---|---|
| • Vibrations induced by the track | - Axle load (train weight and wheel axle spacing)<br>- Geometry of the train<br>- Speed of the train |
| • Wheel-rail interface | - Eccentricity, imbalance, flats, unevenness of the wheel<br>- Bouncing, rolling, pitching, properties of bogie and motor<br>- Acceleration and deceleration of the train |
| • Irregularities on the rail | - Quality of the rail (corrugations, corrosion, unevenness, waviness, joints)<br>- Curves and tiling track |
| • Variations in support structure | - Geometry and stiffness of the support structure (sleepers, ballast and ground)<br>- Frost. |

All of these effects cause train to induce ground-borne vibration. However, in the scope of this thesis vibrations due to irregularities on the rail are to be investigated owing to their random nature.

## 1.3 SCOPE OF THESIS

The scope of this thesis is about modeling ground-borne vibrations from underground rail vehicles using finite elements. Parametric studies are also designed to investigate to the effects of the parameters which have important roles in ground-borne vibration. In this thesis the finite element model is developed based on two models, namely, the original model by Forrest and Hunt [8,11] and the modified one by Sarıgöl [5]. Necessary modifications and underlying assumptions are also outlined in the development phase.

It is aimed to obtain vibration levels of the modeled system within the frequency range of interest as specified by the standards and legislation. Also, a transient analysis to predict the development of vibrations under moving load by the train is sought to complement vibration information obtained in frequency domain.

The finite element model enables the designer to get results faster and to understand the effects of parameters onto resulting ground-borne vibrations in detail.

The thesis attempts to present the material in five chapters in the following order:

Second chapter summarizes the relevant literature in the field upon a brief introduction to the subject in the first chapter. Literature review is organized under headings of rail and track models, models for elements of

components of track such rail pad, floating slab; tunnel model, soil model, vehicle model, and models for excitation.

The modeling approach which consists of finite element modeling is introduced in Chapter 3. Previous models for underground railway systems are also exemplified and discussed in detail.

Case studies and running examples of relevance are presented in Chapter 4. Results of parametric studies are discussed with emphasis on real life applications.

Finally, summary of results, conclusions drawn from the study and recommendations for future work are presented in Chapter 5.

# CHAPTER 2

## LITERATURE SURVEY

In this chapter, a detailed literature survey has been given. The objective of this chapter is to justify the methodology used in this thesis by studying previously works done in literature. The main focus will be given to modeling of the railway system components.

### 2.1 RAIL TRACK MODEL

Railway or railroad is the permanent way which is used by trains. Traditionally, the railways consist of two main parts, permanent way and track foundation. Permanent way consists of rail, sleepers and ballast. Rails are supported on concrete sleepers with fasteners and laid on ballasts. Track foundation consists of subballast and subgrade. The soil or natural ground covers subgrade at the outside. (Figure 2.1)

Different track types are used in the industry. Traditionally, ballasted tracks are used and the main advantages of ballasted tracks are their low construction costs and high vibration damping [3].

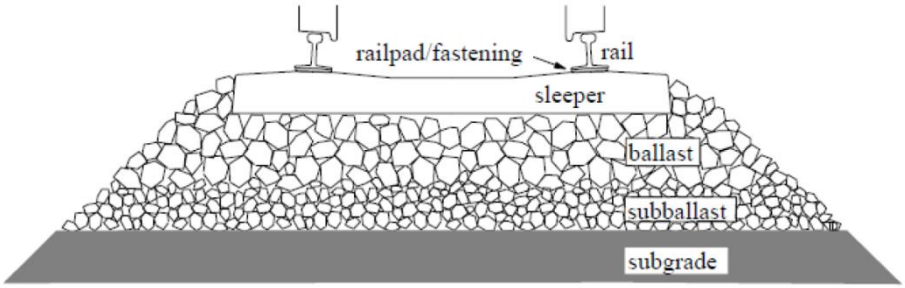


Figure 2.1 Section through railway track and foundation [4]

There are also other kinds of tracks which are often used in urban areas. Especially, ballastless track is very popular due to advantages in maintenance with respect to traditional track. According to the Diehl et al. [1], ballastless track has an advantage on ballasted track, since it has higher sound emissions. The reasons of higher sound emission are the reduced connecting impedance for rail, reduced vibration decay rates and reduced absorption.

A continuous concrete slab is used instead of ballast with this type of ballastless track. An elastic layer is often placed between slab and rail to reduce the vibration.

However, according to the study done with ballast and non-ballast tracks by Galvin et al. [28], the ballast and non-ballast, slab track and floating slab track, systems are compared. It is shown that the soil response is dominated by quasi-static excitation for ballast track and by rail-wheel unevenness excitation for non-ballasted track.

In one of the studies done by Zhai et al. [29], it is focused on the damping mechanisms in the ballast of train tracks. They introduced shear damping and stiffness to model. This model is compared with field testing and the results are parallel with the measured results. They also show that

the difference between the resonance frequency range of the ballast vibration which is 70–100 Hz by calculation and at 80–110 Hz by measurement.

## 2.2 RAIL MODEL

Rails are the beams which train rolls on. Generally, these asymmetrical I beams are made of cast iron. The cross section of the rail may be different in many places around the world. (Figure 2.2)

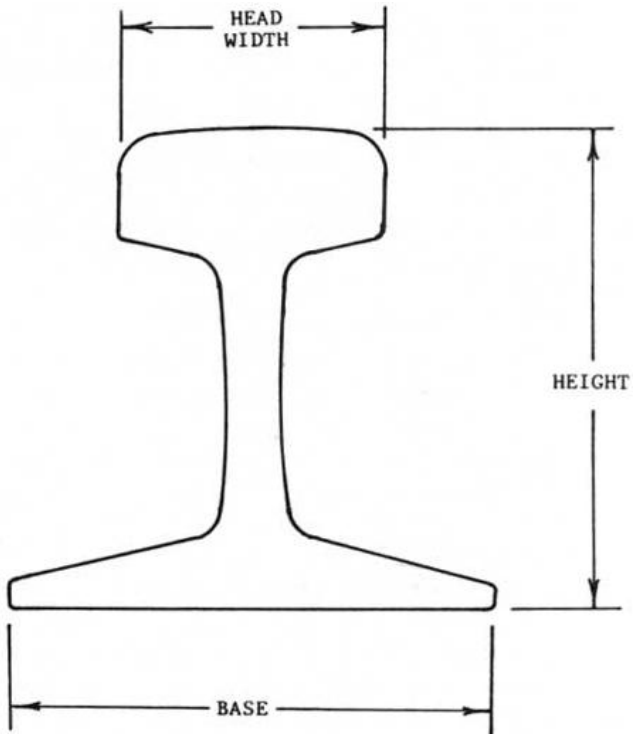


Figure 2.2 Typical rail section [2]

In many studies, rails are modeled as Euler-Bernoulli beams. Especially in early times Euler beam theory is adequate representation of the rail's response to vertical dynamic excitation for low frequencies. It was found that shear deformation of the rail can be neglected only for frequencies below 500 Hz [4]. Therefore, many researchers use this theory in their studies. [1, 8, 11, 14, 15, 16, 17, 18, 19]

The Euler Bernoulli beam example, force acting on it and infinitesimal area are shown in Figure 2.3.

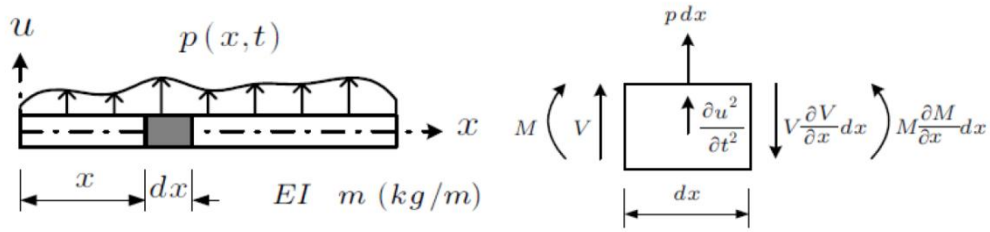


Figure 2.3 The beam is subjected to an external force and has a distributed mass and flexural rigidity which can vary with position and time [4]

Equation of motion of the bending displacement w(x,t) of an Euler beam:

$$EI \cdot \frac{d^4}{dx^4} w(x,t) + \rho A \cdot \frac{d^2}{dt^2} w(x,t) = q(x,t) \tag{2.1}$$

where EI is the bending stiffness or flexural rigidity of the beam, ϱ is the density of the beam, A is cross-sectional area of the beam, q(x, t) is distributed load on the beam and t is time, in SI units.

However, this theory is not sufficient to calculate response to vertical forces at higher frequencies where shear deformations become very important. Later on, a more detailed model known as Timoshenko Beam is developed and applied by researchers to analyze beam transverse vibrations, in particular transverse vibrations of rails [14, 20, 21, 22, 23, 24, 25, 26]. This theory includes rotary inertia and shear deformation of the beam (Figure 2.4).

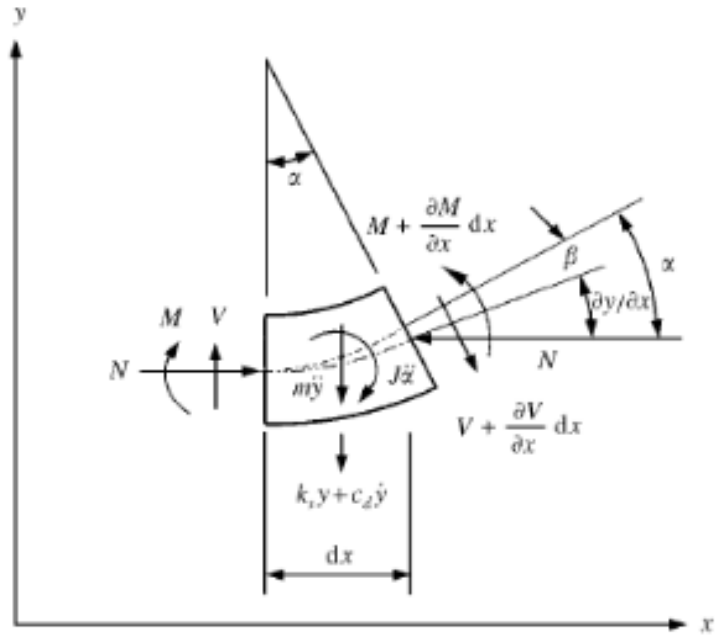


Figure 2.4 A differential Timoshenko beam element [20]

In this theory, the shear deformation is an unknown besides the deflection and the equation of motion becomes as following:

$$EI\cdot\frac{d^1}{dx^1}\omega(x,t)+\rho A\cdot\frac{d^1}{dt^1}\omega(x,t)+\boxed{-\rho I\cdot\left(1+\frac{E}{\kappa\cdot G}\right)\cdot\frac{d^1}{dx^1}\frac{d^1}{dt^1}\omega(x,t)+\frac{\rho^1\cdot I}{\kappa\cdot G}\cdot\frac{d^1}{dx^1}\omega(x,t)}=q(x,t) \qquad (2.2)$$

where *G* is the shear modulus, k is the shear factor, t is time and the dotted area marks differences compared to Euler-Bernoulli beam.

Configurations of Timoshenko beams are used according to the vibration type of interest. If only longitudinal vibrations are investigated, rail can be modeled as a single Timoshenko beam according to Knothe and Grassie [27]; however if the lateral and torsional modes are to be studied; then rail heads and feet are modeled as independent Timoshenko beams connected by rotational springs [5].

## 2.3 RAIL PAD MODEL

The most effective solution for reducing vibration is found to isolate rail-track systems. An elastic element, rail pad is introduced between the supporting foundation and rails providing a mechanical filter. This type of intervention also provides a high degree of damping [3].

The rail pads are generally modeled as spring-damper combination in parallel. Therefore, rail pads can be thought as elastic foundations. (Figure 2.5 and 2.6) Rail pads also have an important role in vibration and since they affect the overall stiffness and stability of the system.

The rail pad stiffness should be as low as possible to a certain limit. In Europe, rail pads having 100-200 MN/m dynamic stiffness and 50-100 MN/m static stiffness are commonly used [4]. These rail pad parameters cannot be found easily; therefore some novel techniques are developed to determine the dynamic properties of rail pads. Remennikov and Kaewunruen [32] study an instrumented hammer impact technique to determine the dynamic properties of the rail pads in Australia. This approach not only tests the new rail pad types but also evaluates the influence of age of pads on their dynamic characteristics.

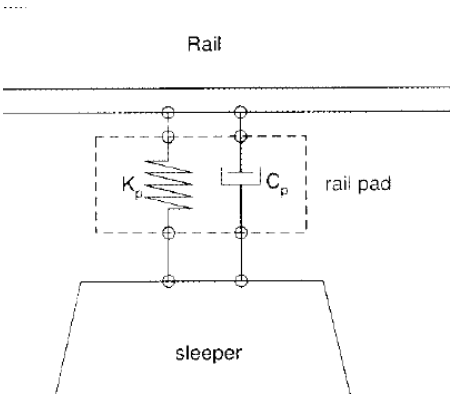


Figure 2.5 Schematic representation of rail pad [32]

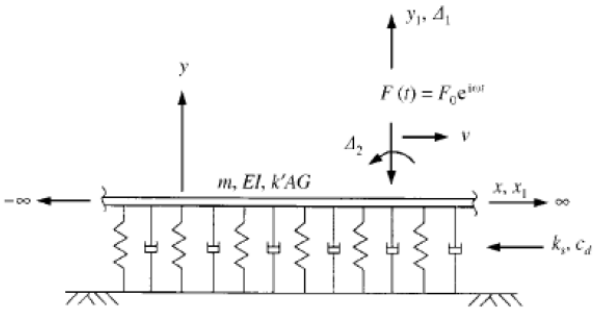


Figure 2.6 Beam on viscoelastic foundation [20]

## 2.4 FLOATING SLAB MODEL

One of the most effective ways to reduce the vibration transmitted from rails to tunnel structure is floating slabs. Slabs can be continuous cast or can be series of precast. Also concrete slab is used in tunnels with rubber bearings to isolate it.

Forrest and Hunt [5, 11] coupled the slab to the tunnel system and it is shown that track slab may increase the transmission of vibration. Also, Galvin et al. [28] show that using floating slab presents vibrations higher than slab system at where frequencies around the isolation frequency. However, a reduction of the response is obtained far from the track.

Lombaert et al. [30] developed a numerical model for the prediction of vibrations with the influence of the floating slab. The free field vibrations are studied and it is shown that the effective reduction in the free field is highly dependent on the dynamic characteristics of the slab and the soil.

## 2.5 TUNNEL MODEL

The tunnel structure has also important role in the vibration. Its material type, thickness and mass as well as the geometry, i.e., the form of its cross-section can affect the transmission of vibration. According to Kurzweil [6] a doubling of the average wall thickness, for the same material, can lead to reductions in the wall vibration levels of 5 to 18 dB. (Table 2.1)

Ideally an underground railway tunnel is modeled as a thin-wall cylinder. Forrest and Hunt [8] developed a three-dimensional model of the

tunnel analytically as an infinitely long, thin cylindrical shell surrounded by soil of infinite radial extent.

In the paper of D. Clouteau et al. [7], the three-dimensional dynamic tunnel–soil interaction problem is solved with a subdomain formulation. The periodicity of the tunnel and the soil in the longitudinal direction is exploited using the Floquet transform, limiting the discretization effort to a single bounded reference cell.

Table 2.1 Effect of subway structure type on tunnel vibration levels [5, 6]

| Subway structure | Relative vibration level (dB) |
|---|---|
| Cast iron or steel single tunnel | +4 |
| Concrete single tunnel or box | +2 |
| Double box | 0 |
| Triple box | -2 |
| Station | -4 |

Andersen and Jones [31] studied two dimensional and three dimensional tunnel models. Although both tunnel models show similar trend in the wave pattern and results agree with each other at most frequencies, the two-dimensional model produces more useable results when the structure is buried in the ground. Therefore, according to this study, two dimensional modeling can be preferable for practical uses unless absolute vibration transmission predictions and more accurate estimates of

the changes in response due to changes in tunnel structure or depth are desired.

## 2.6 SOIL MODEL

Soil is very complex owing to its nonlinear characteristics. Therefore, it forms an important aspect in modeling vibration transmitted to surrounding buildings. According to Gutowski and Dym [5, 33], in order to predict the excitation levels at buildings, one should know how much vibration transmitted through the soil. However, it is difficult to determine the accurate soil properties; thus soil behavior cannot be understood well enough.

Most of the researches model the soil as a half space model. Homogeneous, linear and isotropic model assumption is made for this effort. Picoux and Houédec [34] developed a solution to 3D multi layered half space problem. They used Fourier transform for a semi-analytical solution in the wave number domain. For the steady state solution all equations are written in the wave number domain. After that inverse Fourier transform is applied with matrix equation solution of the whole system.

In the study of Jones et al [35], the ground is modeled as an elastic half-space also. In order to get the transformed solutions, double Fourier transform is used. Numerical results for the displacements on the surface are presented for loads moving with speeds up to the Rayleigh wave speed of the ground.

Hung and Yang [36] studied elastic waves in viscoelastic half space generated by various vehicle loads. In this paper, a viscoelastic half space is

subjected to various moving loads with static and dynamic components. Four loading types are investigated. In each case, the influence of the moving loads traveling in the subsonic, transonic and supersonic ranges on the dynamic responses of the half-space is studied. Therefore, results about the mechanism of wave propagation for a viscoelastic half space under moving loads are obtained.

In the study of Sarıgöl [5], it is mentioned that the ballast and the soil can be considered together as elastic or viscoelastic half-space. On the other hand, a layer of ballast on three dimensional half space models can also be used (Figure 2.7). However, the theoretical investigation of this model is very difficult. The ballast and soil (subtrate) can be modeled by eliminating the discrete sleeper support. This condition requires modeling the ballast as vertical springs and dashpots in parallel per unit length.

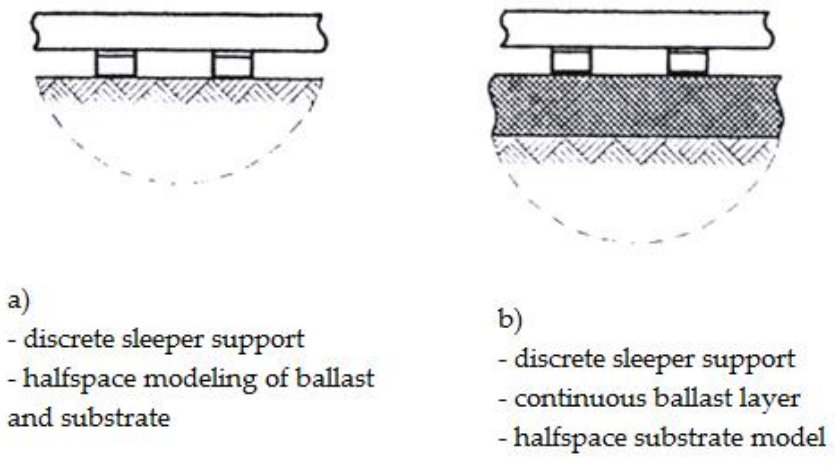


Figure 2.7 a) Half space modeling of ballast and subtrate b) ballast layer half space model [5]

In another paper, by Chupin et al. [37], the response of a viscoelastic layered half space to a moving load with interlayer slip was obtained by semi analytical method. The influence of the interface sliding condition on the response of a layered viscoelastic half space was addressed through an application dedicated to pavement structures. The analysis was conducted on the longitudinal strain ($\varepsilon_{xx}$) and the normal stress ($\sigma_{xx}$). For interlayer slip, normal stress in the viscoelastic layers decreases as load speed decreases whereas normal stress in the elastic layer increases.

The main difference between the viscoelastic and the elastic half space model lies in the applied damping model [5]. Lefeuve-Mesgouez et.al [38] investigated about this damping in their model. The model consists of an elastic, isotropic and homogeneous half-space, with modified hysteretic damping. Modified Lame constants $\mu$ and $\lambda$ are used in damping predictions.

Underground railway tunnel can also be thought of as a thin-walled cylinder and soil can be thought as a thick-walled cylinder outside the tunnel. (Figure 2.8)

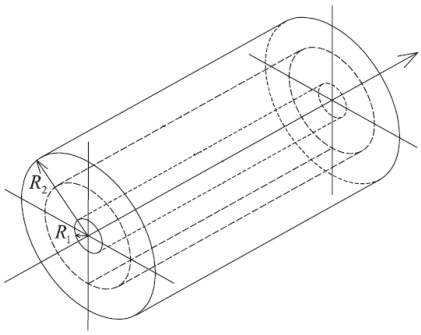


Figure 2.8 Inner pipe representing the tunnel modeled as a thin-walled cylinder (left) and outer pipe representing the soil with outer radius $R_2$ goes to infinity (right) [8]

## 2.7 VEHICLE MODEL

Traditionally, a rail vehicle body rests on two bogies which contain two wheelsets. Bogie is a framework carrying wheels, attached to the vehicle and wheelset is the wheel axle assembly of a rail vehicle. There are also springs and damping elements in a vehicle. The set of elements which are used to connect the wheelset and bogie, are called primary suspension while other sets which are used to connect bogie and the main body, are called secondary suspension. (Figure 2.9)

In the paper of Gialleonardo et al. [40], a multi-body model was defined for one single vehicle with standard architecture, composed by one car body resting on two bogies and four wheelsets. The car body and bogies are modeled as rigid bodies, since their effect on wheel–rail contact forces is confined to the low frequency range, due to the effect of the primary and secondary suspensions. On the other hand, wheelset flexibility may significantly affect the high-frequency component of wheel–rail contact forces. Therefore, two wheelset models with increasing complexity were defined: the first considering the wheelsets as rigid bodies and the second taking into account wheelset flexibility.

At low speeds the response is quasi-static so that the track response due to train axle loads appears mostly downward at the point of their action. On the other hand, at high speeds the train-induced response becomes dynamic due to the inertia generated in the track–ground system, so that the track vibrations appear evenly in both upward and downward directions. [5]

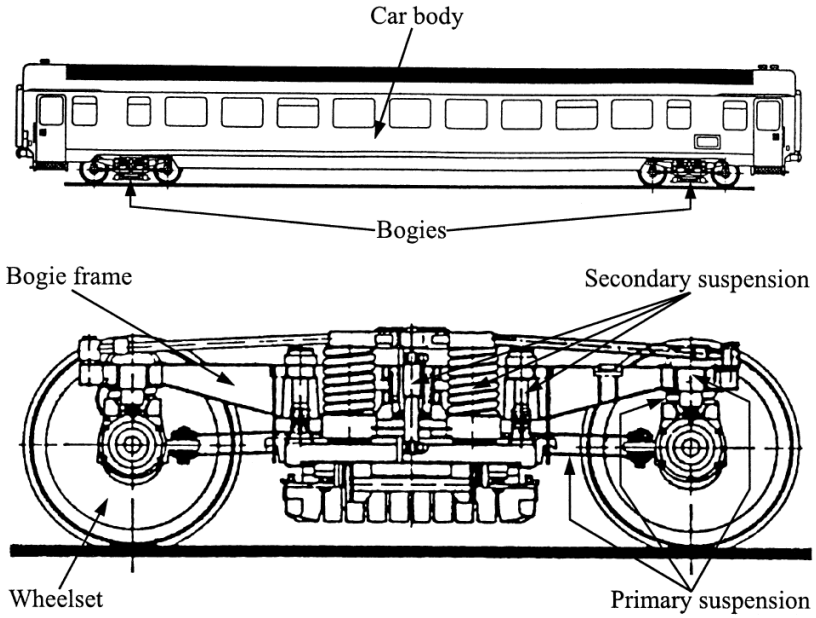


Figure 2.9 Components of vehicle with primary and secondary suspension [39]

Hou et al. [22] discussed a 10 degree-of-freedom vehicle model. A two level suspension vehicle model is employed. The wheelset and the bogie are connected by the primary suspension while the car body is supported on the bogie through the secondary suspension. A more realistic vehicle model incorporating two wheelsets, two bogie side frames, and half a car body is represented as a 10-d.o.f. model. Each wheelset has vertical and rotational DOF at its center ($u_{w1}$; $u_{w2}$; $\theta_{w1}$ and $\theta_{w2}$). The bogies have vertical ($u_{B1}$ and $u_{B2}$) and pitch ($\theta_{B1}$ and $\theta_{B2}$) DOF while the car body has vertical ($u_c$) and rotational ($\theta_C$) DOF. (Figure 2.10)

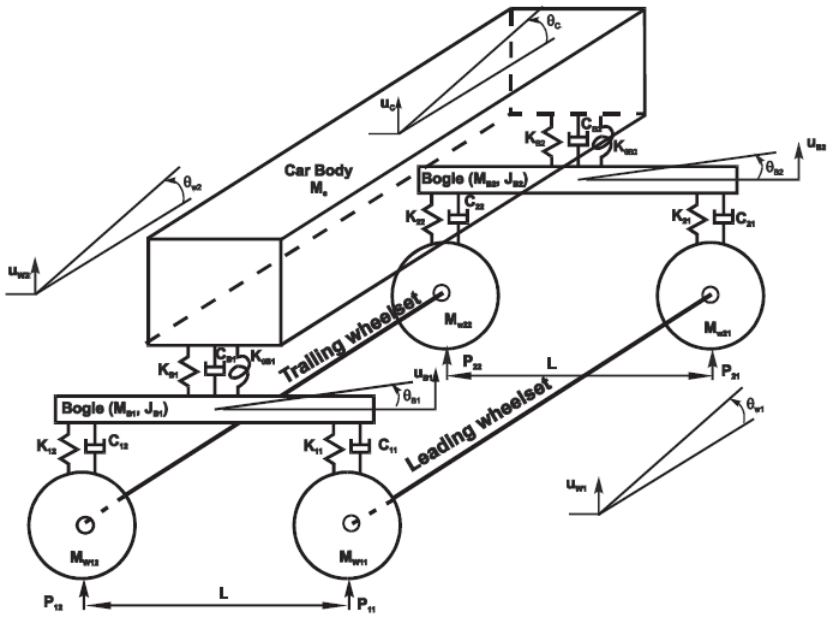


Figure 2.10 Ten degree of freedom vehicle model [22]

In the paper of Zhang et al. [26] a 35 degree-of-freedom system was investigated. Similarly, the passenger car considered in their study is equipped with a pair of two-axle bogies with double suspension systems. The wheelset and the bogie are connected by the primary suspension, while the carriage is supported on the bogie through the secondary suspension. For convenience, the front bogie and rear bogie are numbered 1 and 2, respectively, the leading and trailing wheelsets of the front bogie are numbered 1 and 2, respectively, and the corresponding wheelsets of the rear bogie are indicated by 3 and 4. Therefore, total degree of freedom of the rail vehicle is 35 while the longitudinal motions of the vehicle are ignored. These degrees of freedoms are outlined in Table 2.2.

Table 2.2 Degrees of freedom of the vehicle [26]

| Vehicle Component | Type of motion | | | | |
|---|---|---|---|---|---|
| | Lateral | Vertical | Roll | Pitch | Yaw |
| Wheelset 1 | $Y_{w1}$ | $Z_{w1}$ | $\phi_{w1}$ | $\beta_{w1}$ | $\psi_{w1}$ |
| Wheelset 2 | $Y_{w2}$ | $Z_{w2}$ | $\phi_{w2}$ | $\beta_{w2}$ | $\psi_{w2}$ |
| Wheelset 3 | $Y_{w3}$ | $Z_{w3}$ | $\phi_{w3}$ | $\beta_{w3}$ | $\psi_{w3}$ |
| Wheelset 4 | $Y_{w4}$ | $Z_{w4}$ | $\phi_{w4}$ | $\beta_{w4}$ | $\psi_{w4}$ |
| Front bogie frame | $Y_{b1}$ | $Z_{b1}$ | $\phi_{b1}$ | $\beta_{b1}$ | $\psi_{b1}$ |
| Rear bogie frame | $Y_{b2}$ | $Z_{b2}$ | $\phi_{b2}$ | $\beta_{b2}$ | $\psi_{b2}$ |
| Car body | $Y_{c}$ | $Z_{c}$ | $\phi_{c}$ | $\beta_{c}$ | $\psi_{c}$ |

## 2.8 EXCITATION MODELS

If the system is vibrating, there must be a kind of excitation. Causes of these excitations are mostly wheel-rail discontinuities and track irregularities.

### 2.8.1 Wheel Rail Discontinuities

Sun and Dhanasekar [23] claims that the main reasons can be attributed to the vibration is discontinuities in wheel and rail or unround wheels. Irregularities in wheel and/or rail generate sharp peak responses. Some irregularities cause periodic excitation while others cause non-periodic or localized excitation. The periodic irregularities include the rail corrugations, the out-of-round wheels or the rounded flat wheels as shown in Table 2.3.

Table 2.3 Sources of harmonic excitations [23]

| Name and geometry | Expression |
|---|---|
| Out-of-round wheel 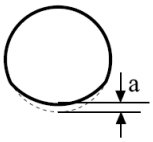  | $W_d(t) = a(1 - \cos \Omega t)/2$<br>$\Omega = \frac{2\pi V}{L_d}$<br>$(0 \leqslant t \leqslant L_d/V)$ |
| Indentation on rail surface 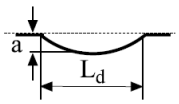  | $a$—wave length of irregularity<br>$L_d$—wave depth of irregularity<br>(for out-of-round wheel, $L_d$ is the length of arc) |

Periodic irregularities are represented by cosine functions. Periodic excitations and corresponding expression $W_d(t)$ are shown. On the other hand, non-periodic irregularities include the indentation on the railhead due to the spalling or the defect of welded joint and the dipped-joint, shown in Table 2.4.

Table 2.4 Sources of impulse excitations [23]

| Name and geometry | Impulse velocity |
|---|---|
| Raise on welding joint 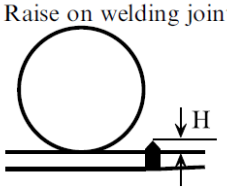  | $V_0 = V(\frac{2H}{r})^{1/2}$<br>$r$—wheel radius<br>$V$—wagon spped |
| Dipped-joint 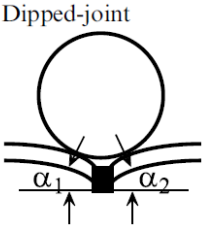  | $V_0 = (\alpha_1 + \alpha_2)V$<br>$\alpha_1$, $\alpha_2$—dip angles of joint |

When the excitation source is non-periodic and $L_d \leq 2\sqrt{2ra - a^2}$ ; where $L_d$ is the wavelength of irregularity, r is the rolling radius of wheel, a is the wave depth of the irregularity, the wheel and the rail will not be in contact with the trough of the irregularity. For small $L_d$, when the flat wheel runs on the perfect rail or the perfect wheel runs at the defective rail, the instantaneous rotating center of the wheel suddenly moves down or up, inducing a vertical impact velocity. In this situation, these excitation sources are called as the impulse excitation sources.

In the paper of Michaltsos and Raftoyiannis [41], combined effect of an existing rail discontinuity on the dynamic behavior of the bridge is taken into account with different train speeds. According to this study, it is seen that in all bridge cases where a rail discontinuity is present, the amplitudes increase further, by the order of 20% to 150%, due to the imposed impact loading. Therefore, it must be avoided placing rail discontinuities near the mid-span of the bridge.

### 2.8.2 Track Irregularities

Small amplitude fluctuations with a broad spectrum of wavelengths are present on the running surfaces of wheels and rails [42]. These irregularities lead to a broadband relative displacement excitation of wheel and rail, inducing high-frequency vertical wheel–rail contact forces accompanied with vibrations and rolling noise.

In the paper of Sheng et al. [43], a model was developed for predicting ground vibrations due to vertical track irregularities serving as input excitations. A relationship is derived between the vertical rail irregularity spectral density and the ground vibration power spectra. This

relationship means that predictions from the model can be presented in terms comparable to actual vibration measurements.

According to the Suhairy [44], dynamic forces arise between the wheel and the rail due to irregularities of the surface and wheel. (Figure 2.11)

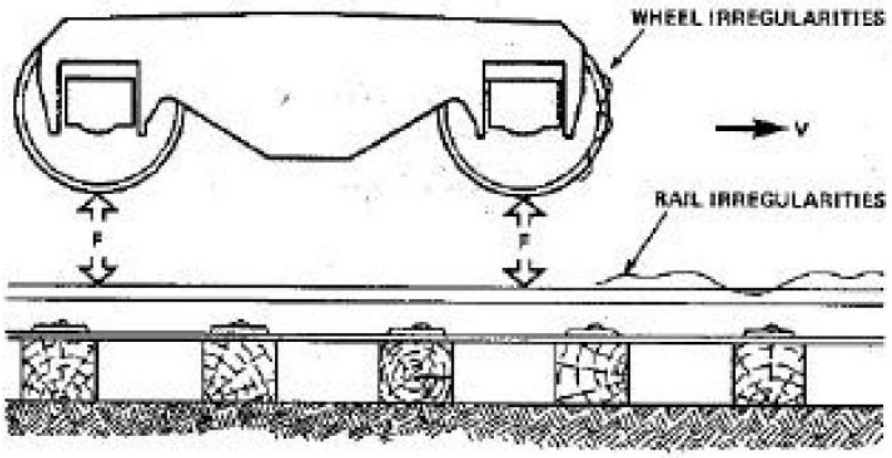


Figure 2.11 Wheel-rail interaction [44]

The rail response velocity, $V_R$ , is shown to be proportional to the wheel, $Z_W(\omega)$ and the rail, $Z_R(\omega)$ impedances [44].

$$V_R \propto \frac{Z_W(\omega)}{Z_W(\omega) + Z_R(\omega)} \tag{2.3}$$

$Z_W(\omega)$ and $Z_R(\omega)$ are the vertical point impedances of the wheel and the rail respectively. It should be noted that $Z_W(\omega)$ is not just the impedance of the wheel but includes the influence of the axle, the bogie, the car body,

and bogie suspension elements. The most effective impedance was found to be the wheel impedance $Z_W(\omega)$ [44].

Track irregularities are also caused by factors such as small imperfections in materials, imperfections in manufacturing of rails and rail joints, terrain irregularities, and errors in surveying during design and construction. In practice, the roughness excitation is composed of unevenness on the wheel and rail contact surfaces having a broadband spectrum over a range of wavelengths. Since irregularities of different wavelengths are due to different independent factors, irregularity can be treated as a random function. Unevenness on the wheel and rail contact surface and the axle loads of the vehicles are often described as a stationary random process [5].

Lei and Noda [45] considered the track vertical profile irregularity as stationary ergodic Gaussian random processes. Power spectral density function, $S_X(\omega)$, is used for numerical simulation of the random irregularity of track vertical profile.

The formulation of the irregularities in terms of power spectral density function is presented as:

$$S(\omega) = \frac{kA_v\omega_c^2}{(\omega^2 + \omega_c^2)\omega^2} \tag{2.4}$$

where $A_v$ and $\omega_c$ are coefficients associated with line grade, as shown in Table 2.5, and k is a constant, normally equal to 0.25.

Table 2.5 Coefficients for $A_v$ and $\omega_c$ [45]

| Line Grade | $A_v$ ($cm^2$ rad/m) | $\omega_c$ (rad/m) |
|---|---|---|
| 1 (worst) | 1.2107 | 0.8245 |
| 2 | 1.0181 | 0.8245 |
| 3 | 0.6816 | 0.8245 |
| 4 | 0.5376 | 0.8245 |
| 5 | 0.2095 | 0.8245 |
| 6 (best) | 0.0339 | 0.8245 |

In the study by Forrest and Hunt [11], Frederich's formula [50] for rail irregularity power spectral densities based on many measurements of the track geometry of different surface railways was used. The spatial power spectral density of track irregularity is given by the single-sided spectrum:

$$S_\delta(\tfrac{1}{\lambda}) = \frac{a}{(b+\tfrac{1}{\lambda})^3} \tag{2.5}$$

where $\lambda$ is the irregularity wavelength, a is an ''unevenness'' parameter and b is a ''waviness'' parameter.

The conversion of Equation 2.5 to a function of frequency is shown below:

$$S_{\delta}(f) = \frac{a}{v(b + f/v)^3} \tag{2.6}$$

where f is the frequency in Hz, v is the train speed [km/h], a is an ''unevenness'' parameter and b is a ''waviness'' parameter again. The values of the unevenness a and waviness b are given in Table 2.6 by Frederich [50].

Table 2.6 Values of the unevenness a and waviness b of vertical railway track irregularity, for three different track conditions [11].

| | $a(mm^2.(1/m)^2)$ | $b(1/m)$ |
|---|---|---|
| Worst | $9.39X10^{-1}$ | $6.89X10^{-2}$ |
| Average | $1.31X10^{-2}$ | $2.94X10^{-2}$ |
| Best | $1.90X10^{-4}$ | $9.71X10^{-3}$ |

## 2.9 CONTACT MODELING

It is well known that the contact modeling is very essential issue. There are two main types of models. One represents a wheel rolling over roughness on the rail. The other is a moving irregularity model. Moving irregularity model can be regarded as the one in which the wheel remains in a fixed position on the rail, and a strip combining the roughness on the

wheel tread and railhead is effectively pulled at a steady speed between wheel and rail. For rolling noise modeling, this moving irregularity model has been widely used.

In Figure 2.12, a roughness is pulled between a stationary wheel and the rail. Wheel and track are considered as linear whereas contact stiffness is considered as non-linear in the system.

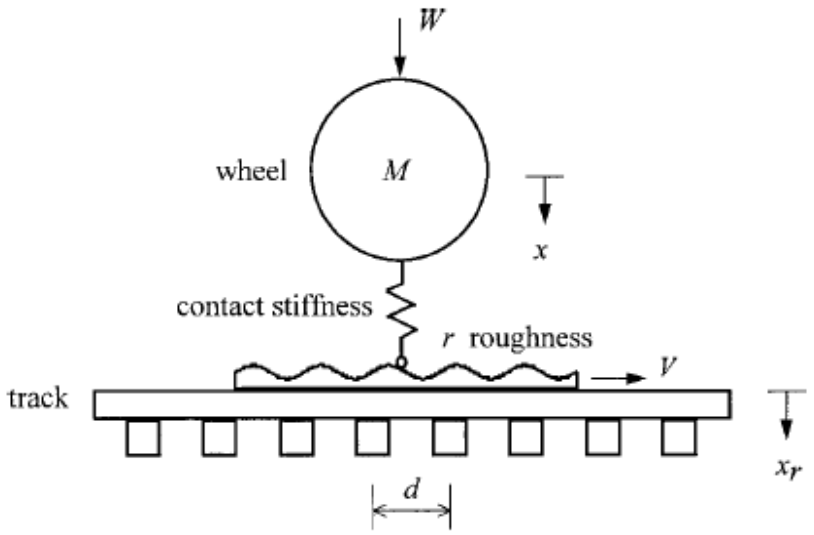


Figure 2.12 Moving irregularity model [5]

For a linear system, which is not time varying, the equation of motion can be expressed in the frequency-domain. In a simple case of vertical interaction between wheel and rail, the contact force $F$ can be given as in [5, 46].

$$F(\omega) = -\frac{R(\omega)}{\alpha^W(\omega) + \alpha^C(\omega) + \alpha^R(\omega)} \tag{2.7}$$

where $R$ is the relative displacement (roughness) between the wheel and rail; $\alpha^W$, $\alpha^C$ and $\alpha^R$ are the point receptances (displacement divided by force) of the wheel, contact spring and rail respectively and $\omega$ is the circular frequency of the excitation (roughness).

The representation of a non-linear wheel/rail contact force is proportional to the contact deflection to the power 3/2, which is given below [5, 46]

$$f = C_H(x_\omega - x_r - r)^{3/2} \tag{2.8}$$

where $f$ is the wheel/rail contact force, $x_w$ and $x_r$ are the wheel and rail displacements, respectively, $r$ is the roughness, $C_H$ is the Hertzian constant.

Wu and Thompson [47] studied non-linear interaction between rail and wheels and compared the results with linear models. Moving irregularity model was used in their study and the difference between the non-linear and linear interactions is found to be small if the roughness level is not extremely severe and a typical static contact preload exists. The difference increases for low preloads or for high roughness amplitudes. Differences between the linear and non-linear models are found to occur when the r.m.s. roughness amplitude is more than 0.35 times the static deflection of the contact zone; significant loss of contact occurs at amplitudes about 1.5 times greater than this.

In order to make calculations easier and faster, the non-linear wheel/rail dynamic interaction model can be approximated using an equivalent linear model if the roughness level is not so high and also if a moderate static preload is applied to keep the wheel and rail in contact.

## 2.10 FINITE ELEMENT MODELS

As the technology develops, the computer programs have been used widely to solve problems faster and more accurately. Finite Element Method involves dividing up a very complicated problem into small elements that can be solved in relation to each other. Therefore, the problem becomes simple and can be solved faster. Also some cases which are nearly impossible to solve by hand can be solved by such software.

Gardien [14] conducted a study with finite element analysis. In this study, element size, soil stiffness, damping, boundary conditions and finite element method (FEM) software have been varied. Although vibrations generated by a train travelling in a tunnel are of three dimensional (3D) nature, a complete 3D FEM model that contains all aspects is not currently feasible because of required excessive computer power. As it is seen in Figure 2.13, the tunnel model is modeled in finite element software. At the vertical plane along the tunnel axis, symmetrical boundary conditions apply. Infinite boundary conditions apply at the bottom and on the left-hand side. These boundary conditions allow the seismic energy to disappear from the model without reflections, so that the model behaves like an infinite layered half-space.

In the paper of Galvin et al. [28] a general and fully three dimensional multi-body-finite element-boundary element model was used.

The vehicle is modeled as a multi-body system, the track, in both cases, using finite elements and the soil is represented using boundary elements.

Wang et al. [48] assumed a Maglev train to consist of multiple rigid bodies and the magnetic force between the train and its guideway is simulated using linear springs and dampers. The guideway, tunnel and soil are modeled by three dimensional finite elements with perfect match layer as the artificial boundary condition. (Figure 2.14)

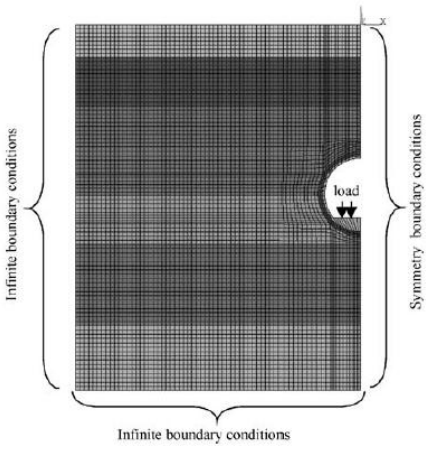


Figure 2.13 Propagation model [14]

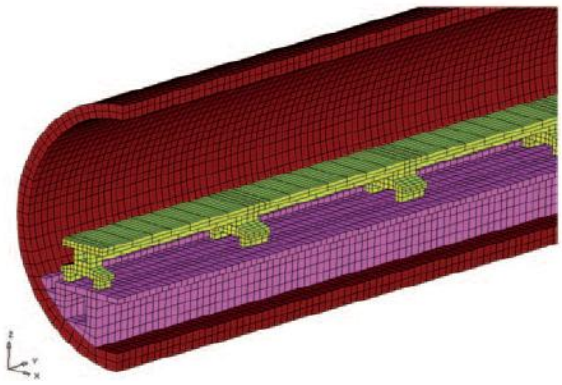

Figure 2.14 Model of the guideway–tunnel–ground system [48]

According to Hall [49], two-dimensional models could be used in order to study certain effects of train-induced ground vibrations. However, three-dimensional analyses are necessary to achieve a detailed simulation of the problem. The three-dimensional model (Figure 2.15) , measured 23 x 65 x 50 $m^3$ and consisted of 98,919 elements and 94,010 nodes. The average element size in the upper part of the model was about 0.65 m in both width and height. Six-node linear brick elements were used in the model. Beam elements for representing the rail were placed 0.7 m from the symmetry line. At a depth of 9 m below the embankment surface, the height of the elements was gradually increased from 0.65 to 8 m at the bottom. The average element size in the model was calculated to be 1.10 m. The model was set to 65 m in total height.

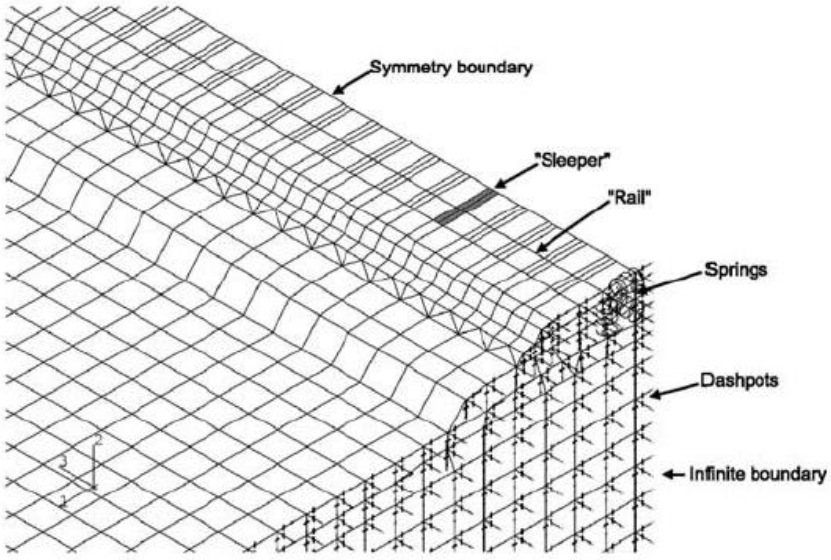


Figure 2.15 Detail of the three-dimensional finite element model [49]

# CHAPTER 3

# MODELING

In this chapter, modeling details for the problem are clarified. The model is based on the approach given by Forrest and Hunt [8, 11] to evaluate vibration velocity at a point in the soil. Firstly, the original and the modified model as described by Sarigol [5] are mentioned. Then, the finite element model is discussed.

## 3.1 ORIGINAL MODEL

Forrest and Hunt modeled the tunnel as thin cylindrical shell with infinite length and with soil of infinite radial extent (Figure 3.1). Inertia terms are added to Flügge equations to obtain the equation of motion for the thin cylindrical shell. Wave equations for an elastic continuum are used to model the homogeneous isotropic soil around the tunnel. A point load is presented in order to obtain the response of the tunnel. The floating slab track is modeled as a beam and the rails are modeled as beams and they are coupled to the slab beam. It consists of a simple slab beam supporting a rail beam (representing the two rails together) with masses placed at intervals to represent the axle–wheel assemblies of a train.

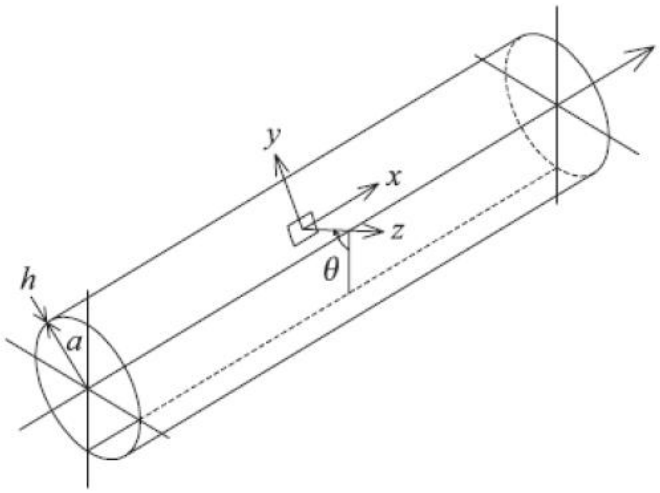


Figure 3.1 Coordinate system for the tunnel and soil around the tunnel, tunnel radius -a, the tunnel wall thickness -h [8]

The slab and rail beams are considered infinitely long. The axle masses are a first approximation train model which only considers the unsprung mass of the train based on the assumption that the primary suspension isolates the rest of each vehicle in the train. Also neglected is the Hertzian contact spring between each wheel and the rail, as it only plays a role at frequencies higher than those of interest.

Full track was modeled with added masses to represent axles of the train. (Figure 3.2) The center of mass is excited by a roughness displacement input δ. The tunnel's infinite length means the responses at one point in the soil to each axle input (paths with dashed lines) are equivalent to the line of separate responses to the single input shown (paths with solid lines) for an infinite number of masses at regular spacing.

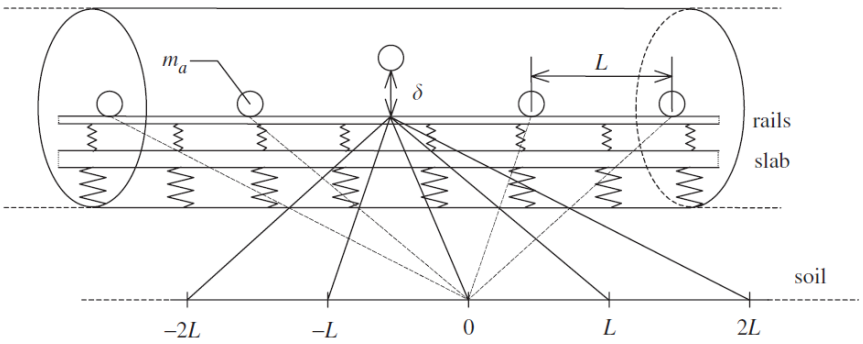


Figure 3.2 Full-track model supported on the tunnel invert [11]

Irregularities are randomly distributed and their effect is interpreted by random process theory. The response of the points in the soil around the tunnel is calculated using the random vibration theory. According to Frederich formula [50], unevenness, a, waviness, b, values are taken as representative of average condition (Table 2.6).

Results are obtained for various train speeds, different radii inside the soil, different orientations inside the soil and velocity components in vertical, longitudinal (train movement) and transverse directions.

## 3.2 MODIFIED MODEL

In the modified model, instead of axle masses, 1/8 car model is used. The 1/8 car mass, $m_c$, bogie mass, $m_b$, the wheel mass, $m_w$, the suspension elements between the bogie and the wheel, $k_1$ and $c_1$, and between the car and the bogie, $k_2$ and $c_2$, are the elements of the 1/8 car model (Figure 3.3)[5].

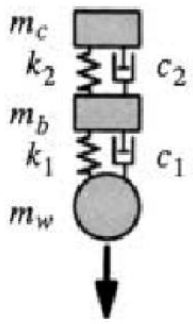


Figure 3.3 Vehicle model with one contact point [51]

According to the specified parameters above, dynamic stiffness matrix relating the vertical displacement of the wheel and loading applied to the wheel, $k_w(w)$ can be calculated as below: [51]

$$k_w(w) = \frac{1}{\frac{1}{k_s(w)} + \frac{1}{iwc_1 + k_1}} - w^2 m_w \tag{3.1}$$

The dynamic stiffness matrix for the bogie is $k_s(w)$:

$$k_s(w) = \frac{1}{\frac{1}{k_c(w)} + \frac{1}{iwc_2 + k_2}} - w^2 m_b \tag{3.2}$$

The dynamic stiffness matrix for the car mass is $k_c(w)$:

$$k_c(w) = -w^2 m_c \tag{3.3}$$

Also the train wheels are not spaced at equal distances for all the wheels. The roughness level in wheels and rail is assumed not to be extremely severe and the nonlinear interaction between the wheel and rail is approximated with an equivalent linear model.

## 3.3. MODEL CONSTRUCTION

In this thesis, two software packages are used in order to model moving train on the rail track in a tunnel. The logic behind the modeling is as following:

First of all, the rail track, slab beam, tunnel and soil are modeled in ANSYS. After modeling, the stiffness matrix can be obtained from ANSYS with substructuring analysis [54]. This stiffness matrix is used in force calculation according to the formula of Forrest and Hunt [11]. The force calculation is performed in MATLAB environment [55]. Once the forces are obtained, then Transient Analysis option is run in ANSYS. This analysis enables maximum vibration velocities to be obtained from desired nodes. Finally, another simple MATLAB code makes the post-processing and presents the results.

The model is based on the following track configuration as shown in Figure 3.4.

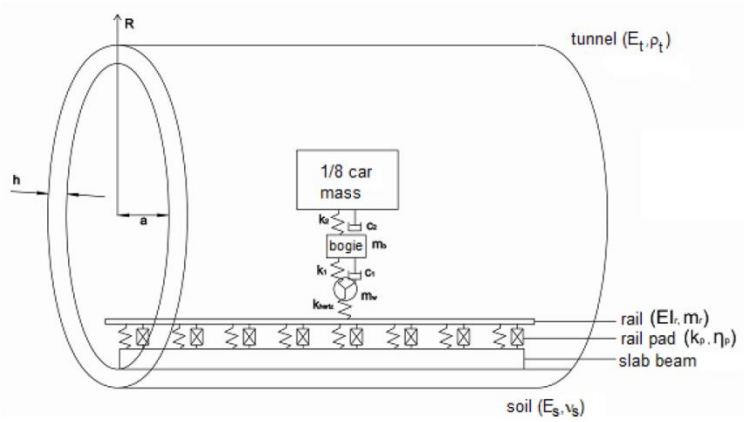


Figure 3.4 Track configuration for Kadıköy-Kartal Line with slab beam used in the model [52]

### 3.3.1 Rail Modeling

In order to model the rail, element type must be selected with respect to analysis criteria and a pre-defined or custom defined cross section is needed. Rail cross section needs to be defined as there is no standard library for rail cross section in ANSYS. In the model, the rail cross section is drawn in CATIA and imported to ANSYS (Figure 3.5).

The other step is choosing the appropriate element type for rail track. While element type is being selected, there are some aspects that must be considered. The computation time is one major concern. On the other hand the accuracy of the analysis is another major issue. Therefore, it must be selected according to analysis criteria.

In this thesis, BEAM188 element is used for modeling the rail. The element is based on Timoshenko beam theory. This element is 2-Node beam element in 3D (Figure 3.6) and it is based on linear, quadratic or cubic shape functions. If linear shape functions are used, one point of integration along

the length is used and all element solution quantities are constant along the length. Two points of integration are used, resulting in linear variation of element solution quantities along the length where beam element based on quadratic shape functions. Similarly, three points of integration along the length are used, resulting quadratic variation of element solution quantities along the length for using cubic shape functions.

### 3.3.2. Rail Pad Modeling

It is assumed that rail track is lying on infinite springs for modeling rail pads. Therefore, spring damper element COMBIN14 is used to simulate the rail pad (Figure 3.7). The spring-damper element has no mass and it can be used as longitudinal option which is a uniaxial tension-compression element. The longitudinal spring element stiffness acts only along its length.

### 3.3.3. Slab Modeling

The slab is modeled with SOLID185 element. This element is used for 3D modeling of solid structures. It is defined by eight nodes having three degrees of freedom at each node. The geometry and material properties of the slab are taken from Kadikoy-Kartal tunnel cross-section. SOLID185 is suitable for modeling general 3D solid structures. It allows for prism and tetrahedral degenerations when used in irregular regions.

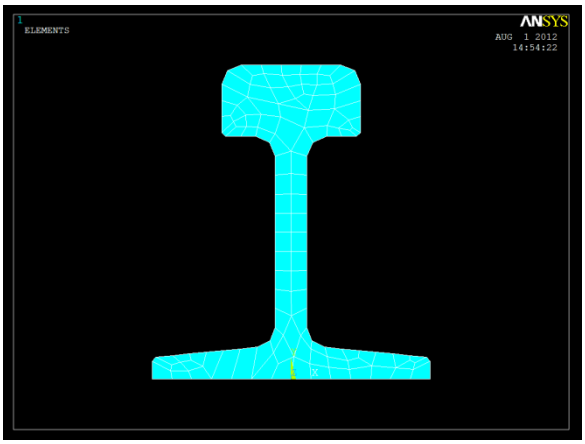


Figure 3.5 Cross section of UIC 54 created in ANSYS

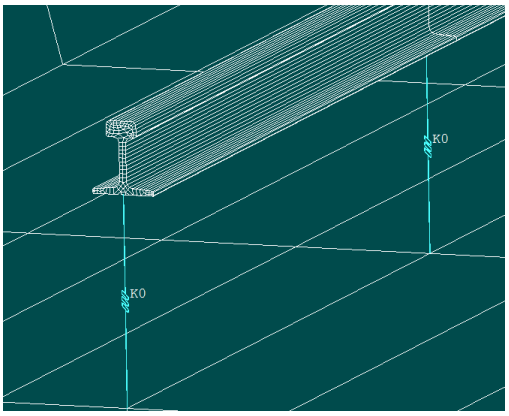


Figure 3.6 Rail track is created by using BEAM188 element

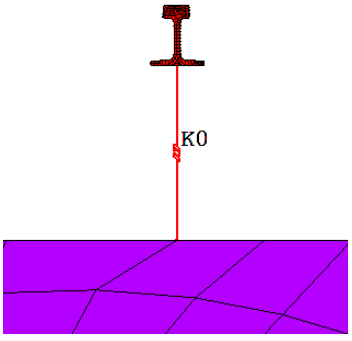


Figure 3.7 Rail is connected to slab with COMBIN14 spring element

### 3.3.4. Tunnel Modeling

Similarly, the tunnel is modeled with SOLID185 element like slab and it is modeled like a cylindrical shell. Same material properties of the slab beam are used in modeling of the tunnel. The most important point is the contact type of the tunnel and the slab beam. In this model it is assumed that there is a perfect contact between tunnel and slab beam (Figure 3.8). No contact element is defined between tunnel and slab beam.

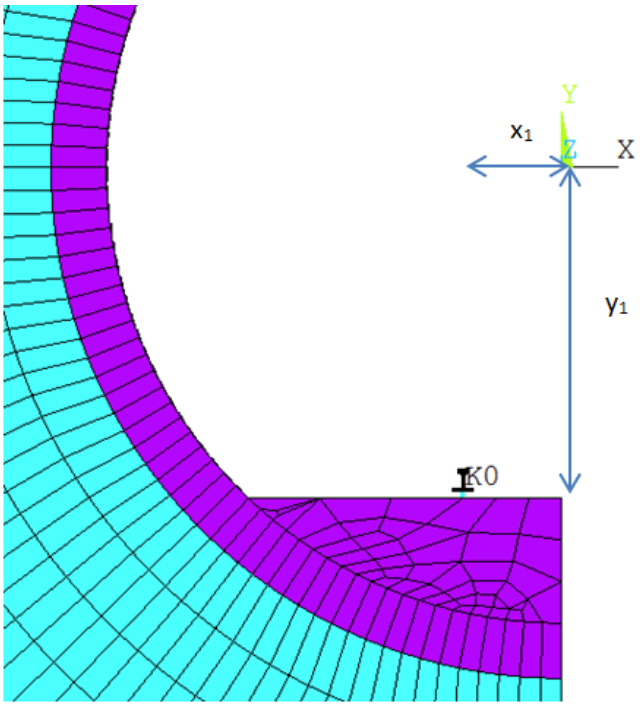


Figure 3.8 Tunnel and slab beam are modeled by SOLID185, where x1 is 717.5 mm and y1 is 2395.38 mm

### 3.3.5. Soil Modeling

Soil is modeled as thick hollow cylinder and SOLID185 is used in modeling with different material properties than slab beam. Soil is modeled as a thick cylinder to decrease the boundary condition effects. Normally, the soil and tunnel are modeled as co-centric cylinders; however, the model is going to be symmetrical and only half of the model is given due to its axisymmetrical characteristics.

### 3.3.6 Meshing and Boundary Conditions

Meshing is the most important process in a finite element analysis, since it directly determines the accuracy of the results. In order to mesh the 3D body easily, PLANE183 element is used. First of all, the cross section of the soil, tunnel and slab are created in 2D. Then, by using PLANE183 element, it is meshed in 2D. After meshing, with the "extrude" command, the cross section becomes a 3D model. Then, PLANE183 element is deleted since it is no longer needed.

The three dimensional model, shown in Figure 3.9 consists of 245881 elements and 353910 nodes. The length of the tunnel is 66 meters and the radius of the tunnel is 53.7 meters (50 m for soil thickness + 3.3 m for tunnel inner radius + 0.4 m for tunnel thickness). The maximum element size does not exceed 0.6 meters in first 10 meters radially. The meshing increments increase as radially going out of the semi-circle in order to reduce computational times. The maximum element size is calculated according to the fact that model must have 6 elements for each wavelength corresponding to the maximum frequency of interest.

The computational time with provided criteria above takes about 1.5 hours for a single frequency, i.e., one Hertz. The range of interest is 1-80 Hz; therefore, it takes 120 hours, i.e., 5 days, for one soil type on quadcore high performance computers.

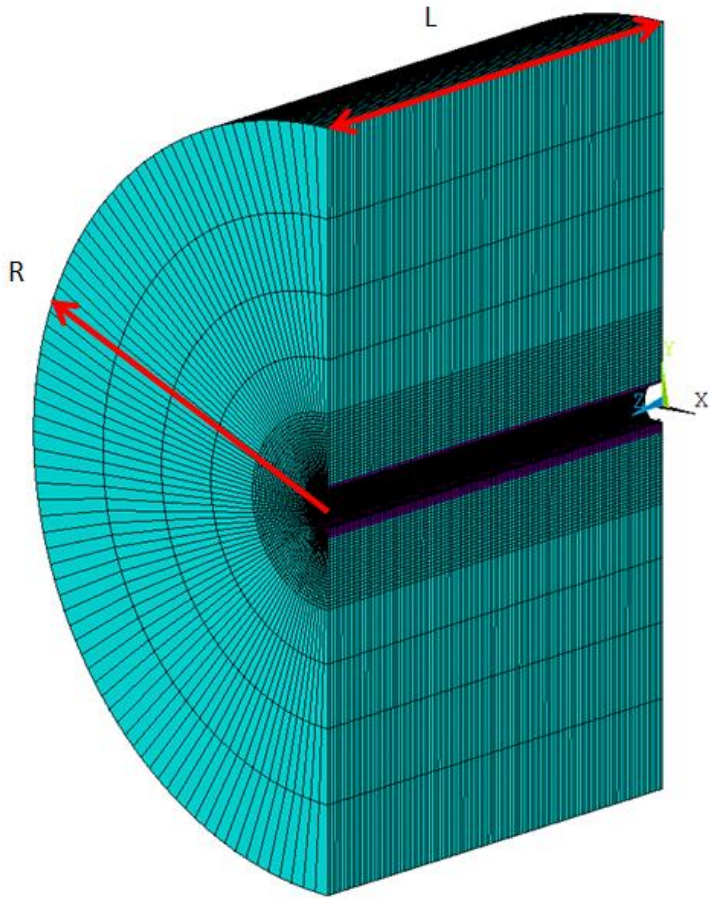


Figure 3.9 Meshing of 3D model with R is 53.7 m and L is 66 m

In this model, it is desired to observe the propagation of the vibration in the soil. Therefore, the propagating waves must not be reflected, i.e., free

space propagation. In order to ascertain this two options can be followed. One of them is to employ fixed boundaries. However, soil is thick enough where most of the vibration energy is lost. The other alternative is to use infinite boundary conditions. In this model the soil thickness is selected according to this criteria but it is also compared with infinite boundary case. Two boundary conditions are applied separately. Firstly, the outer surface of the soil is fixed and secondly the damper elements are introduced at the nodes on the outer surface of the soil and the model has adopted infinite boundary conditions. In addition, only half space model is incorporated to reduce processing times through use of symmetrical boundary conditions (Figure 3.10).

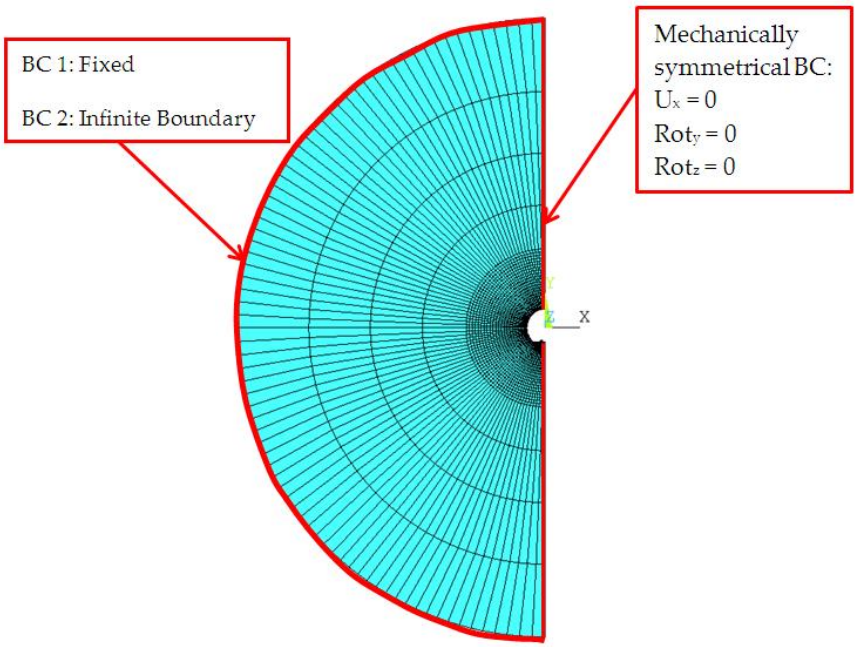


Figure 3.10 Boundary conditions

### 3.3.7 Damping Modeling

ANSYS uses Rayleigh damping in the form of:

$$[C]= \alpha[M] + \beta[K] \tag{3.4}$$

where $\alpha$ is the viscous damping component, and $\beta$ is the hysteresis or solid or stiffness damping component. If alpha damping is ignored, $\beta$ can be calculated from a known value of $\xi$ (damping ratio), which is $\eta/2$, and a known frequency range of $\Delta\omega$.

$$\beta = 2\ \xi/\Delta\omega = \eta/\ \Delta\omega \tag{3.5}$$

As only railpad stiffness and loss factor are made available (Table 4.1) for railpad 1, Equation (3.5) is used for COMBIN14 element. Maximum frequency of interest is taken as 80 Hz, since the interested range is 1 Hz to 80 Hz in the assessment studies.

Also a damping and stiffness values, which are used before in literature [53], are used in order to compare the results.

## 3.4 FORCE CALCULATION WITH RESPECT TO RANDOM PROCESS THEORY

### 3.4.1 Stiffness Matrix

One of the most difficult procedures in model development is building the base model. After modeling, ANSYS can produce the stiffness

matrix of the whole system. This can be achieved by substructuring analysis. However, in this thesis vertical stiffness of the nodes on top of the rail track are interested only, because forces act vertically onto the top of the rail track.

Although ANSYS can yield the stiffness matrix, the elements of the matrix are not ordered. It also gives the unnecessary nodes' stiffness elements due to the modeling and the matrix is not meaningful until it will become an ordered matrix. Therefore, at this point a MATLAB code is written in order to manage the elements of the stiffness matrix. After that step, only the stiffness elements of the desired nodes are obtained in a matrix form for use in force calculation.

### 3.4.2 Force Calculation

In the study by Forrest and Hunt [11], the excitation due to the irregularities on the rail track has been calculated. According to this work, wheels apply an equivalent force on the rail track. While the train is moving at a constant speed, the irregularity of the rail track generates an excitation and it causes an equivalent force to be exerted by each wheel. For that calculation, it is thought that the train is at the middle configuration of the track at that moment; since the middle nodes are taken into consideration to be unaffected or free from boundary conditions due to their distance. In the paper, the logic of the calculation is that the excitation, $\delta$, is applied to every node, respectively. So, a new row and column are introduced in the stiffness matrix. Then, multiplying that matrix with the deflection of each node yields the forces.

The details of force calculation are clarified in 8 steps. It should be noted noted that the numbers and symbols are given as an example to the general approach. The train is assumed to be in the middle of the tunnel.

Step 1 - Obtain stiffness matrix from ANSYS.

The matrix is symmetrical; thus $k_{12}=k_{21}$, $k_{13}=k_{31}$, $k_{23}=k_{32}$ and so on.

$$K = \begin{pmatrix} k_{11} & k_{12} & k_{13} & k_{14} \\ k_{21} & k_{22} & k_{23} & k_{24} \\ k_{31} & k_{32} & k_{33} & k_{34} \\ k_{41} & k_{42} & k_{43} & k_{44} \end{pmatrix} \tag{3.6}$$

Step 2 - Apply displacement to each node.

There are four nodes representing four wheels and a displacement is applied onto each node. Four cases from A to D are shown in Figure 3.11 as

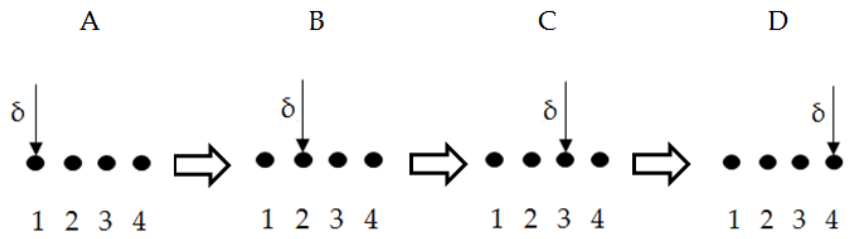


Figure 3.11 Application of displacement to each node

Step 3 – Introduce $k_w$ to the stiffness matrix.

The dynamic stiffness matrix relating the vertical displacement of the wheel and loading applied to the wheel; $k_w(w)$, which can be calculated from Equations 3.1, 3.2 and 3.3, is added to the dynamic stiffness of the system obtained from ANSYS. Therefore, new K matrix, $K_{new}$, is 5x5 now.

For Case A, the displacement is on the first node:

$$K_{new1} = \begin{pmatrix} k_{11} & k_{12} & k_{13} & k_{14} & k_w \\ k_{21} & k_{22}+k_w & k_{23} & k_{24} & 0 \\ k_{31} & k_{32} & k_{33}+k_w & k_{34} & 0 \\ k_{41} & k_{42} & k_{43} & k_{44}+k_w & 0 \\ -k_{11} & 0 & 0 & 0 & k_{11} \end{pmatrix} \quad (3.7)$$

Similarly, for Case B, the displacement on the second node:

$$K_{new2} = \begin{pmatrix} k_{11}+k_w & k_{12} & k_{13} & k_{14} & 0 \\ k_{21} & k_{22} & k_{23} & k_{24} & k_w \\ k_{31} & k_{32} & k_{33}+k_w & k_{34} & 0 \\ k_{41} & k_{42} & k_{43} & k_{44}+k_w & 0 \\ 0 & -k_{12} & 0 & 0 & k_{12} \end{pmatrix} \quad (3.8)$$

For other cases, C and D, $K_{new3}$ and $K_{new4}$ are calculated with similar approach.

Step 4 - Define new displacement and force vectors. Since $\delta = \Delta e^{iwt}$, $k\Delta$ term is added to force vector and $Y_\Delta$ term is added to displacement vector.

For Case A, the displacement vector, Y, and the force vector, F become as in Equation 3.9.

$$Y = \begin{pmatrix} Y_{1A} \\ Y_{2A} \\ Y_{3A} \\ Y_{4A} \\ Y_{\Delta A} \end{pmatrix} \qquad F = \begin{pmatrix} 0 \\ 0 \\ 0 \\ 0 \\ k_{11} \cdot \Delta \end{pmatrix} \tag{3.9}$$

Step 5 – Calculate the displacement amplitude, $\Delta$ [11]

$$\Delta = \sqrt{\frac{1}{v} \cdot \frac{a}{\left(b + \frac{f}{v}\right)^3}} \tag{3.10}$$

where v is train speed in km/h, a is unevenness parameter in $mm^2$ per $m^2$ and b is waviness parameter (1/m) [11] and f is frequency in Hz.

Step 6 - Obtain displacement vector.

As $[K_{new1}].[Y]=[F]$ and both K matrix and F vector are known, the displacement vector can be found easily from the equation below:

$$\begin{pmatrix} k_{11} & k_{12} & k_{13} & k_{14} & k_w \\ k_{21} & k_{22}+k_w & k_{23} & k_{24} & 0 \\ k_{31} & k_{32} & k_{33}+k_w & k_{34} & 0 \\ k_{41} & k_{42} & k_{43} & k_{44}+k_w & 0 \\ -k_{11} & 0 & 0 & 0 & k_{11} \end{pmatrix} \cdot \begin{pmatrix} Y_{1A} \\ Y_{2A} \\ Y_{3A} \\ Y_{4A} \\ Y_{\Delta A} \end{pmatrix} = \begin{pmatrix} 0 \\ 0 \\ 0 \\ 0 \\ k_{11} \cdot \Delta \end{pmatrix} \tag{3.11}$$

Step 7 - Total displacement calculation for excitations applied onto all 4 nodes.

The excitation produces a displacement at each node for every case from A to D and the total displacement is the sum of them.

$$\begin{aligned} Y_1 &= Y_{1A} + Y_{1B} + Y_{1C} + Y_{1D} \\ Y_2 &= Y_{2A} + Y_{2B} + Y_{2C} + Y_{2D} \\ Y_3 &= Y_{3A} + Y_{3B} + Y_{3C} + Y_{3D} \\ Y_4 &= Y_{4A} + Y_{4B} + Y_{4C} + Y_{4D} \end{aligned} \tag{3.12}$$

Step 8 - Obtain force vector.

The force vector can be found from the relation of [K][Y]=[F] where K and Y vectors are known.

$$\begin{pmatrix} k_{11} & k_{12} & k_{13} & k_{14} \\ k_{21} & k_{22} & k_{23} & k_{24} \\ k_{31} & k_{32} & k_{33} & k_{34} \\ k_{41} & k_{42} & k_{43} & k_{44} \end{pmatrix} \cdot \begin{pmatrix} Y_1 \\ Y_2 \\ Y_3 \\ Y_4 \end{pmatrix} = \begin{pmatrix} F_1 \\ F_2 \\ F_3 \\ F_4 \end{pmatrix} \tag{3.13}$$

As it can be seen from equations, calculations are dependent on frequency. Therefore, the procedure must be repeated for all frequencies from 1 Hz to 80 Hz. Consequently, four forces are obtained for each frequency from 1-80 Hz.

## 3.5 ANALYSIS AND POST PROCESSING

After four forces acting from each wheel have been calculated, they are input to run transient analysis mode. Successive wheel placement is like in Figure 3.12, where $L_{w1}$ is 2.2 meters and $L_{w2}$ is 3.91 meters. Therefore, forces are moving on the rail track with this configuration as shown in Figure 3.13.

For each frequency, there are four forces. Therefore, transient analysis must be performed 80 times. After each run, ANSYS captures the maximum vibration velocity values occurred at the middle nodes of the rail, tunnel and soil. The peak vibration velocity values of each frequency are

plotted in MATLAB environment. The vibration velocity change with respect to time is also obtained.

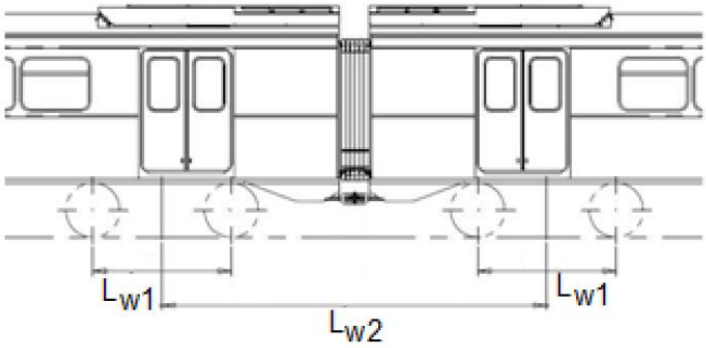


Figure 3.12 Successive wheel spacing [52]

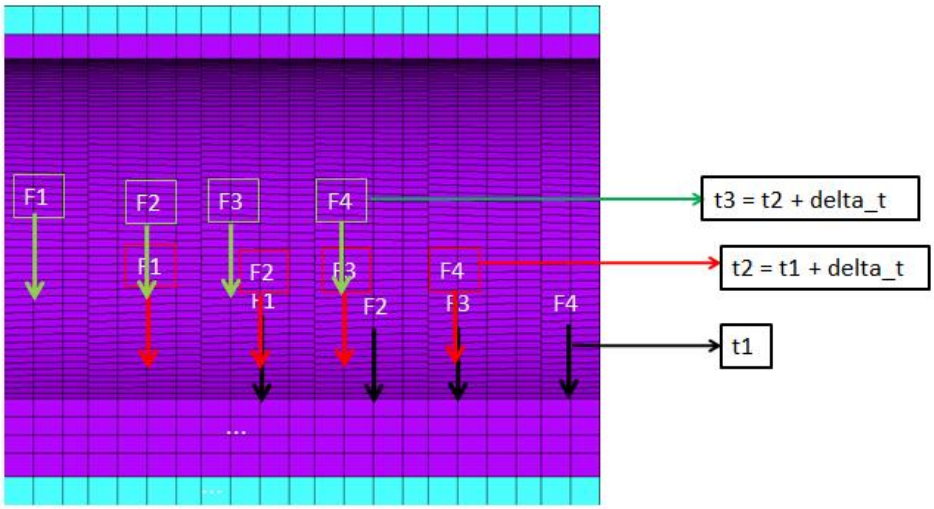


Figure 3.13 Forces moving on the rail track

# CHAPTER 4

## RESULTS AND DISCUSSION

In this chapter, several case studies consisting of parametric studies are designed to study and demonstrate effects of several parameters such as soil type, railpads and train speed. The case studies are conducted on the modified model of the original Forrest and Hunt formulation [8, 11]. The parameters used in this thesis are tabulated in Table 4.1.

Table 4.1 Parameters used in case studies

| **1/8 car model** | **Tunnel** | **Soil Type A** | **Soil Type B** | **Rail Pad (1)** | **Rail Pad (2)** | **Train Speed** |
|---|---|---|---|---|---|---|
| $m_c$=7650 kg | $E_t$=50 x $10^9$ Pa | $E_s$=780 MPa | $E_s$=9800 MPa | $k_r$=1.6 x $10^7$ N/m | $k_r$=120 x $10^6$ N/m | 80 km/h |
| $m_b$=1530 kg | $\nu_t$=0.3 | $\nu_s$=0.29 | $\nu_s$=0.18 | $\eta_r$=0.2 | $c_r$=16 x $10^3$ kNs/m | 100 km/h |
| $m_w$=320.5 kg | $\varrho_t$=2500 kg/m$^3$ | $\varrho_s$=2500 kg/m$^3$ | $\varrho_s$=2700 kg/m$^3$ | | | |
| $k_1$=9.32 x $10^6$ N/m | a=3.33 m | $\eta_g$=0.1 | $\eta_g$=0.1 | | | |
| $k_2$=4.16 x $10^5$ N/m | h=0.4 m | | | | | |
| $c_1$=1.2 x $10^4$ Ns/m | $\eta$=0 | | | | | |
| $c_2$=1 x $10^4$ Ns/m | | | | | | |

Two different types of soil are investigated in the study. Soil A represents the soft soil with low modulus of elasticity and Soil B represents the stiff soil as can be seen from Table 4.1. These soil types are compared on the basis of combinations with railpad type. Railpad 1 parameters are obtained from Kadikoy – Kartal Metro Line. Railpad 2 parameters are taken from reference [53] to vary stiffness and damping values. Therefore, both soil types and railpads are investigated through numerical experiments designed within case studies with respect to their effects on vibration propagation in the soil. On the other hand, the effect of train speed is also studied. All these studies are performed in frequency domain.

In this thesis, transient analysis is performed to see temporal and spatial behavior of vibration within the soil. The vibration propagation is traced in both upward and downward directions (Figure 4.1).

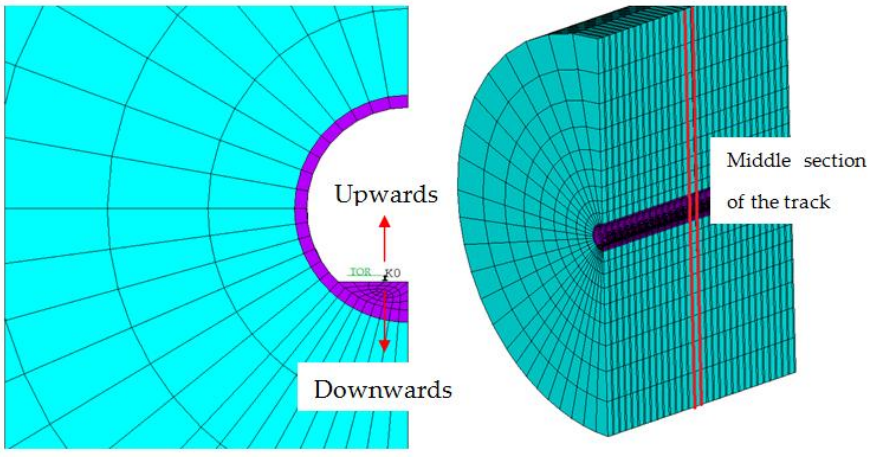


Figure 4.1 Upward and downward directions

## 4.1 RAILPAD 1

Analysis is performed for railpad 1 firstly. Figure 4.2 demonstrates peak vibration velocity as a function of frequency and distance from top of the rail. It is observed that the the peak value of the vibration velocity is much higher in soft soil, soil A than stiff soil, soil B in upward direction from top of rail (TOR).

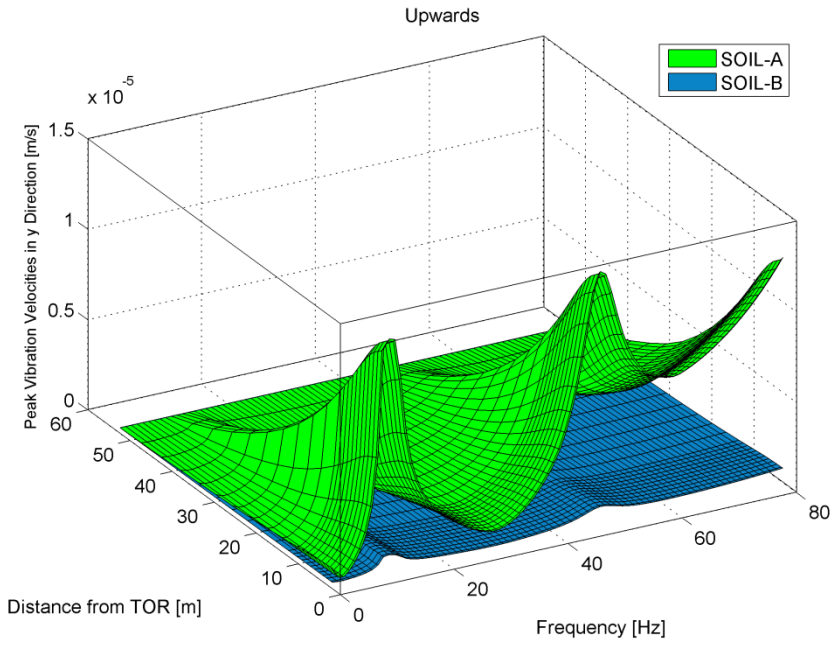


Figure 4.2 Amplitude of peak vibration velocity for a train speed of 80 km/h (Railpad 1)

The difference between these two vibration amplitudes is so high that the effect of the stiff soil can hardly be noticed; therefore, the graph is reproduced in logarithmic scale in Figure 4.3.

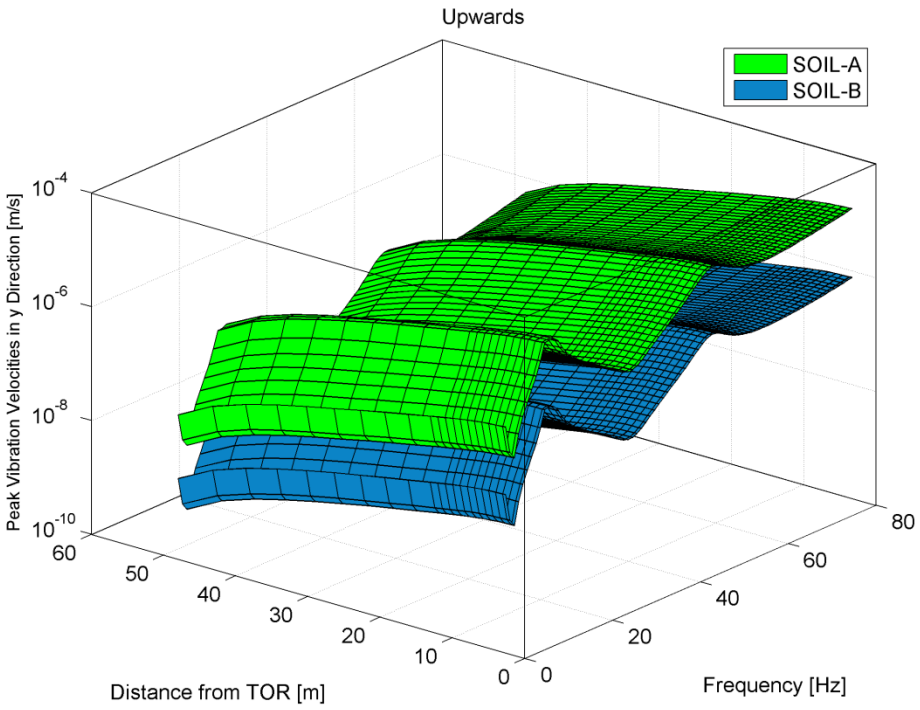


Figure 4.3 Amplitude of peak vibration velocity in logarithmic scale for a train speed of 80 km/h (Railpad 1)

In the Figure 4.3, it is clearly seen that there exist approximately 3 orders of magnitude difference on the average for the whole frequency range between two soil types in favor of the stiff soil B from vibration mitigation standpoint. The general trend is a decrease in amplitudes as the distance from top of rail is increased. This outcome is consistent with the expectations gathered from the related literature. Two peaks around 12 Hz and 48 Hz are singled out in the vibration response while undamped natural frequencies of the 1/8 car model are found to be around 3 Hz and 30 Hz. These peaks are well correlated with the dominant frequencies in applied forcing, i.e., wheel forces (Figure 4.4).

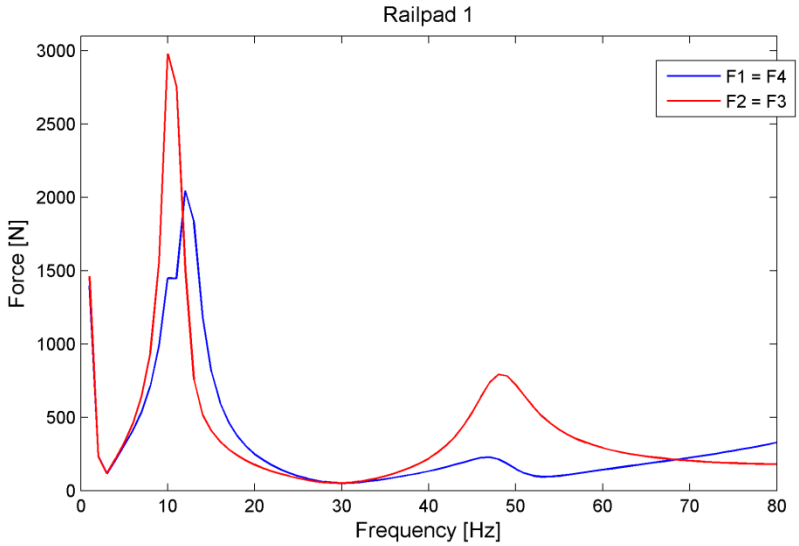


Figure 4.4 Force vs Frequency (Railpad 1)

In the Figure 4.4, the change in forces with respect to frequency can be seen. Although there are four forces, in the graph only two lines are seen as the wheel forces are symmetrical.

Soft soil A is expected to have higher magnitude of vibrations than stiff soil B; however, vibrations in the softer soil, soil A are anticipated to decay faster than stiffer soil B owing to higher damping or energy dissipation characteristics as shown in Figure 4.5. The analysis ends in about 3 seconds, since the train completes its travel along the tunnel within this period. If it is waited enough, soil A will be damped faster than soil E. At the beginning, soil A has sharper increase in vibration behavior than soil B. In the meanwhile, soil A is estimated to have sharper decrease than soil B at the end.

The comparisons of two soil types are plotted in logarithmic scale in Figure 4.6. The green plot belongs to soil A with higher vibration velocity amplitudes. It decreases by 4 orders of magnitude in 50 meters from the top of rail. The other plot colored in blue belongs to soil B decreases by 2 orders of magnitude in same distance.

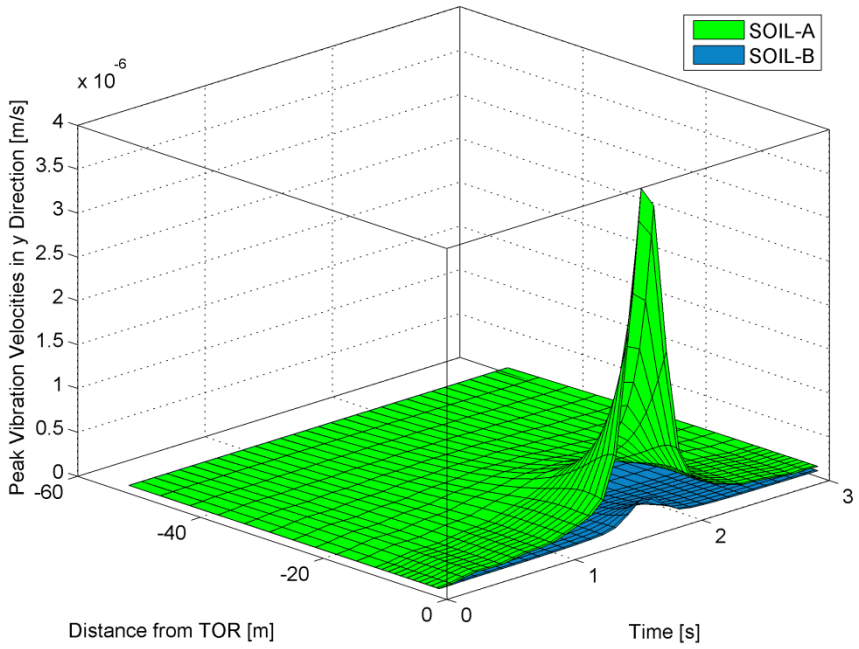


Figure 4.5 Temporal and spatial change in peak vibration velocity for train speed of 80 km/h (Railpad 1)

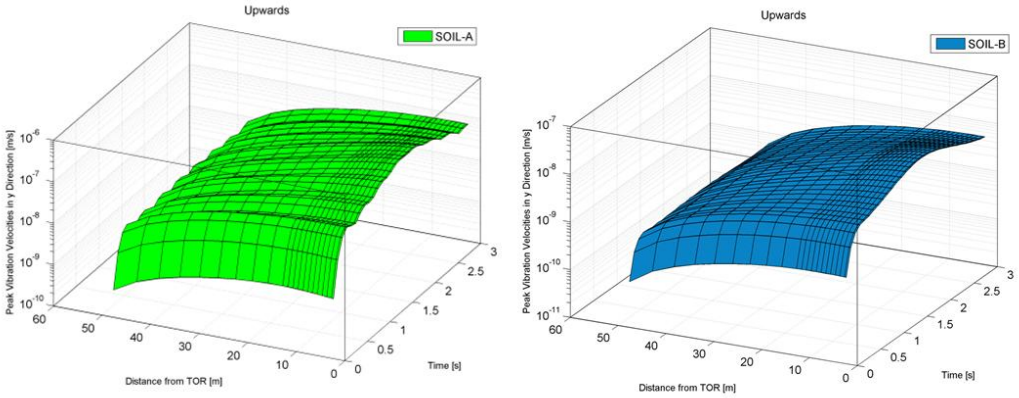


Figure 4.6 Temporal and spatial change in peak vibration velocity in logarithmic scale for train speed of 80 km/h (Railpad 1)

## 4.2 RAILPAD 2

A similar analysis is performed for railpad 2 to perceive the effect of the railpad by means of changing stiffness and damping of the system. Change in vibration velocity in frequency domain is illustrated in Figure 4.7.

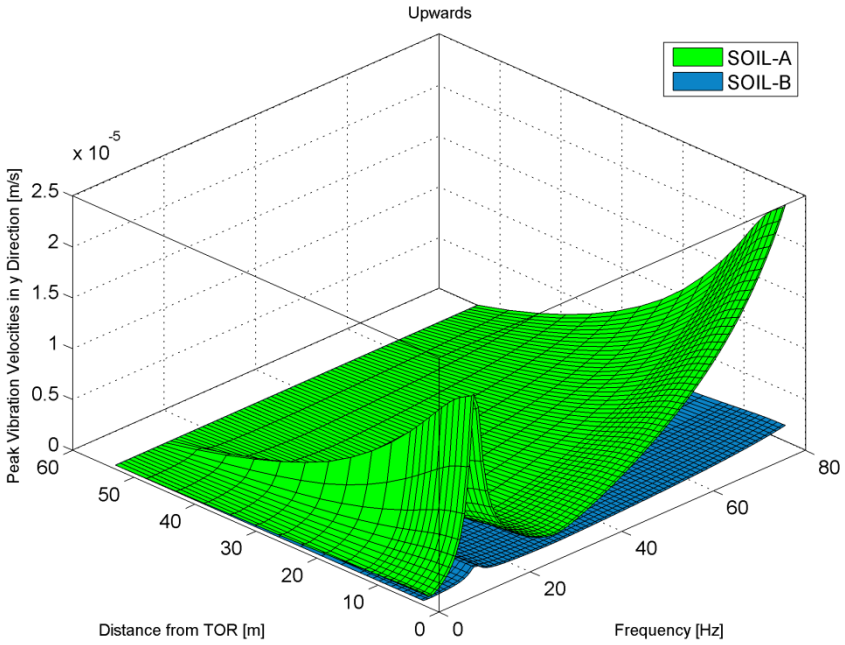


Figure 4.7 Amplitude of peak vibration velocity for a train speed of 80 km/h (Railpad 2)

This figure provides information to see the difference in amplitude of peak vibration velocity within two soil types; however, the difference is so high and the effect of the soil B cannot be comprehended clearly. Therefore, Figure 4.8 which is obtained in logarithmic scale has an advantage of evaluating two soil types in terms of vibration velocities.

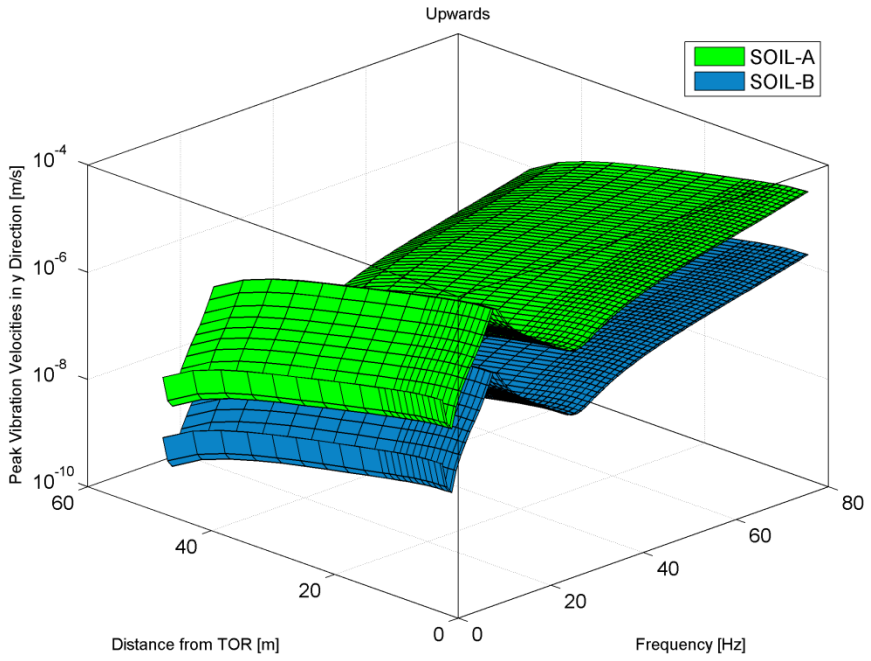


Figure 4.8 Amplitude of peak vibration velocity in logarithmic scale for a train speed of 80 km/h (Railpad 2)

In Figure 4.8, the most important difference from Figure 4.3, which belongs to railpad 1, is that it has only one peak in the frequency domain while Figure 4.3 has two peaks. The reason can be attributed to the stiffness characteristics of this particular railpad. Due to its higher stiffness the second peak may occur out of the interested frequency range. This is justified the increasing tendency of vibration velocity behavior near the high limiting frequency. Actually, the force plot, Figure 4.9, is changed by changing the railpad properties. Force graph shows similarity with Figure 4.8 again as the stiffness matrix of the whole system is changed and it affects the force calculation directly.

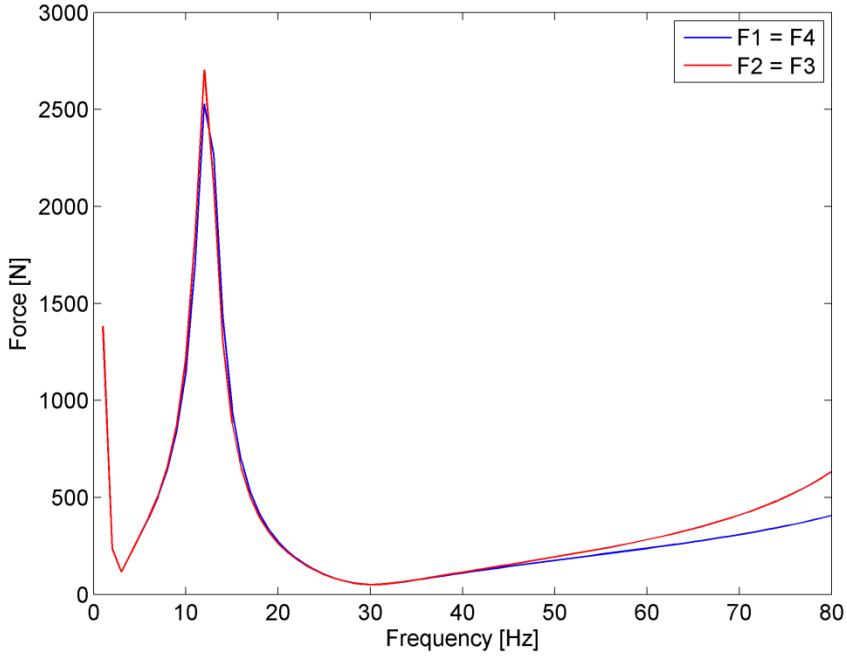


Figure 4.9 Force vs Frequency (Railpad 2)

In the Figure 4.10, vibration velocities are obtained in time domain. Again, the soft soil, soil A has developed much higher vibration amplitudes than that of the stiff soil, soil B. In logarithmic scale, they have similar trends. However, the soil A has a dramatic decrease in magnitude than soil B. They are drawn together in the third graph, but not in logarithmic scale. Plot of Soil A increases and decreases with similar decay characteristics. Plot of Soil B seems smoother than Soil A (Figure 4.5 and Figure 4.6). In the stiff soil the vibration amplitude is not so high whereas it is damped faster within the soft soil.

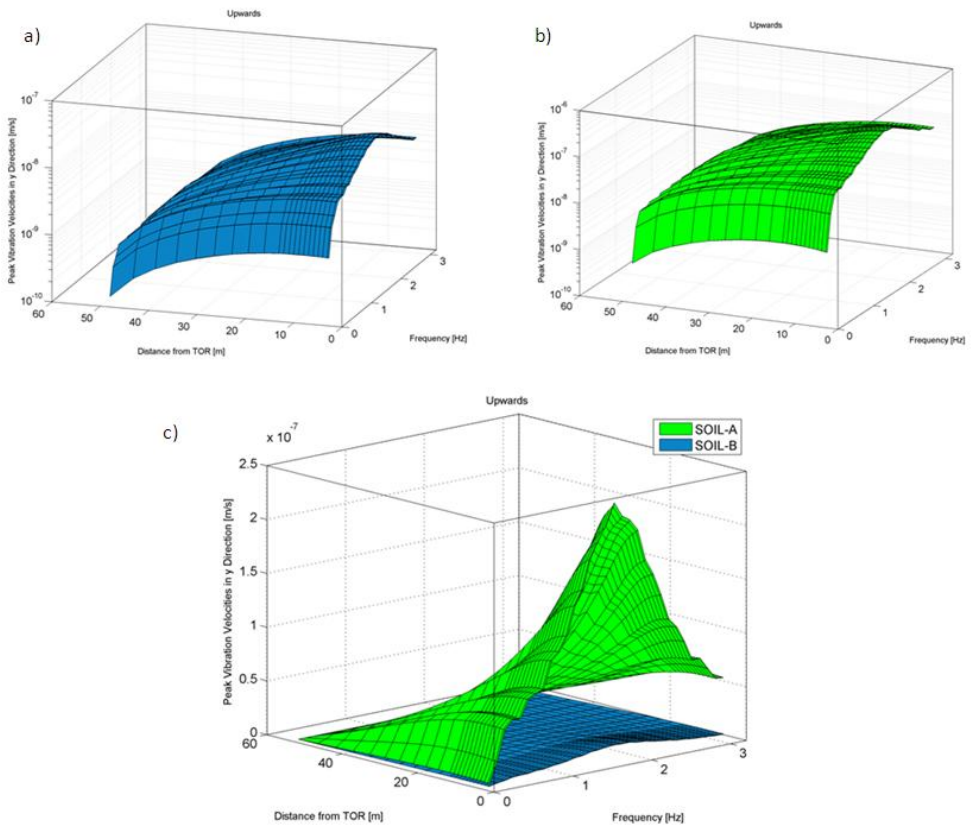


Figure 4.10 Temporal and spatial change in peak vibration velocity in logarithmic scale for train speed of 80 km/h (Railpad 2) a) Soil B b) Soil A (c) Soil A and Soil B Together (not logarithmic scale)

## 4.3 TRAIN SPEED

One of the important factors which affects the vibration level is the train speed. In the study all of the analyses are performed with a train speed of 80 km/h, design speed of Kadıköy-Kartal Metro Line. In this section, it is investigated how the vibration levels change if the train speed increases from 80 km/h to 100 km/h. In Figure 4.11, it is understood that the amplitude of vibration is increased by increasing the train speed. This analysis is performed with railpad 2 and Soil A configuration.

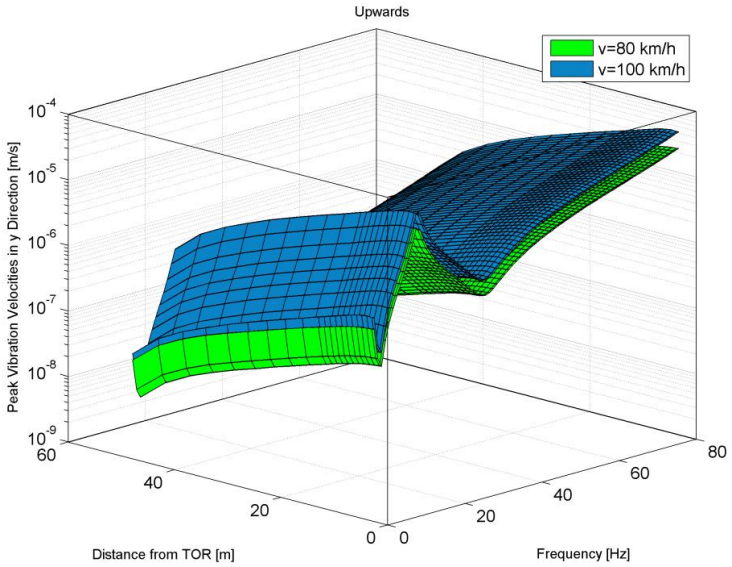


Figure 4.11 Change of peak vibration velocity in logarithmic scale for a train speed 80 km/h and 100 km/h

The peak vibration velocity change is monitored in time domain. In Figure 4.12, transient analysis results for both train speeds are plotted together. Trains with a speed of 100 km/h complete the track in 0.7 seconds earlier than trains with lower speed, typically of 80 km/h. However, the faster train produces higher vibration amplitudes. It may be concluded if the train speed increases, very sharp increases and decreases occur in vibration behavior as the train accelerates in a short time.

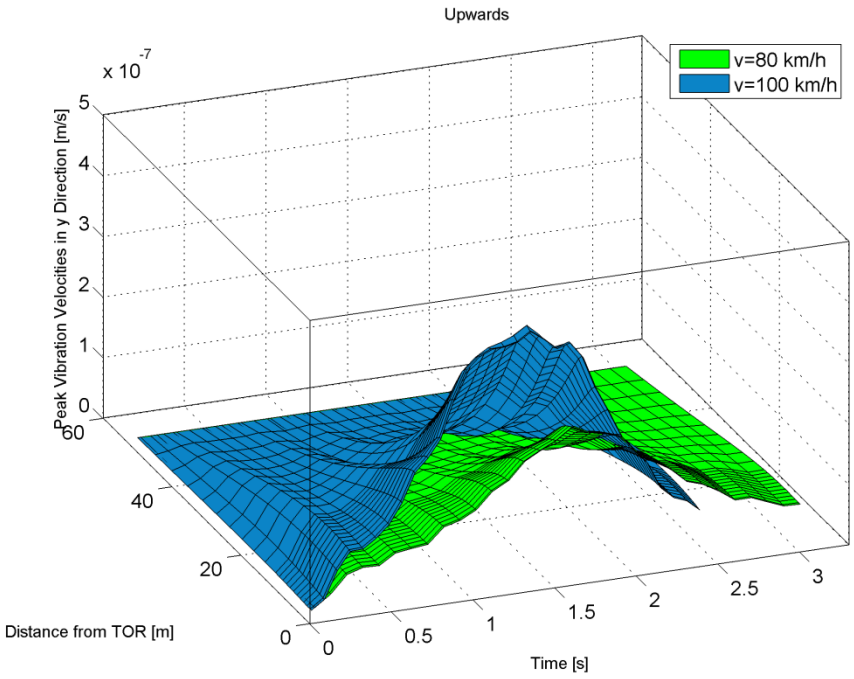


Figure 4.12 Comparisons of train speeds in time domain

## 4.4 OTHER STUDIES

The soil is modeled as a thick hollow cylinder in all these analyses. It is assumed that its thickness is 50 meters and it is fixed from outer surface. It is anticipated that vibrational waves are damped before they reach to the boundary and they are not reflected back. Another study is conducted with infinite boundary conditions to validate this assumption. In this study, damper elements are placed at the outer surface of the soil in every direction. Therefore, the waves can be damped and they are never reflected.

Vibration propagates farther in stiff soil than soft soil; therefore, in this study soil B and railpad 2 configuration is used with a train speed of 80 km/h. In Figure 4.13, it is clearly observed that the two graphs obtained for differing boundary conditions are very close to each other. On the left graph, the vibration change is given in the frequency domain and it is given in the time domain for soil B on the right one. The difference is negligible between the two graphs. Therefore, 50 meters thickness of soil assumption is found to be sufficient for the analyses conducted.

Another study is carried on the direction of the vibration whether it is upwards or downwards. All of the results are obtained for upward direction from top of rail; since the interested region is in the upwards close to the ground level. However, it is also concerned how vibration propagates in downward direction. A case study is designed for this purpose with a configuration of railpad 1 and train speed of 80 km/h (Figure 4.14). It is discovered that vibration amplitudes and changes in these amplitudes are similar. However, in downward direction, vibration decreases faster due to

the proximity of soil to the track. It is hypothesized that the tunnel damps out energy in propagation of vibrational waves in upward direction.

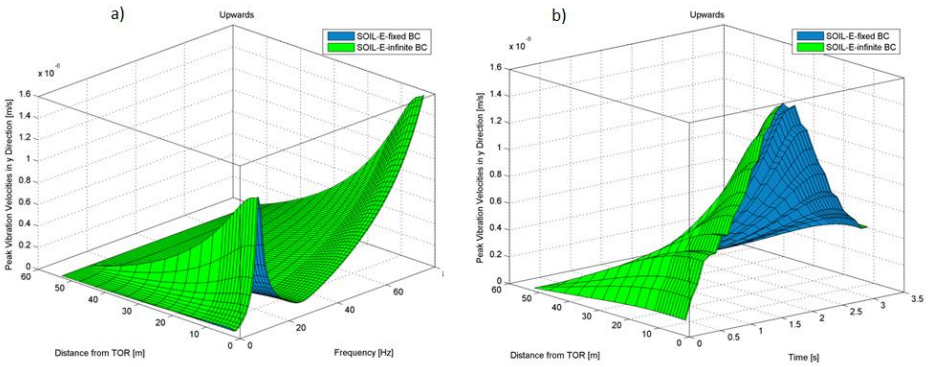


Figure 4.13 Fixed and infinite boundary conditions in a) Frequency Domain and b) Time Domain

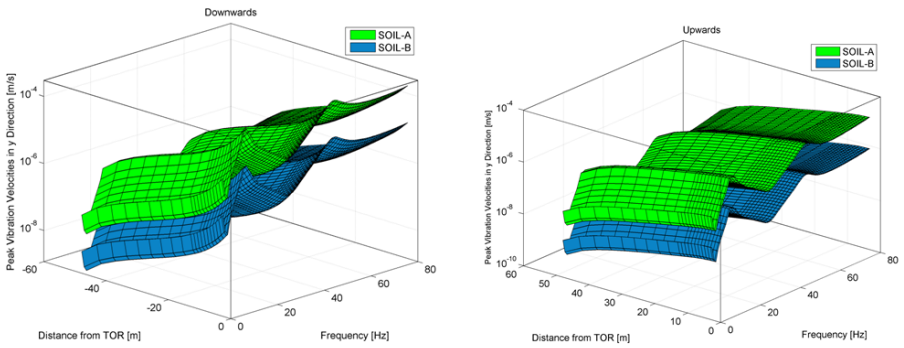


Figure 4.14 Vibration velocity change in downwards and upwards

Final study is conducted to understand how vibration propagates along the tunnel length. This transient analysis yields contour plots for conveniently selected first 12 steps starting from Figure 4.15 to Figure 4.26. There are extra two figures for vibration propagation in the middle and at the end of tunnel as displayed in Figure 4.27 and Figure 4.28, respectively. In the figures, the distribution of the deformation in vertical direction and longitudinal direction. All values are in meters. It is observed that the vibration waves attenuate in upward direction.

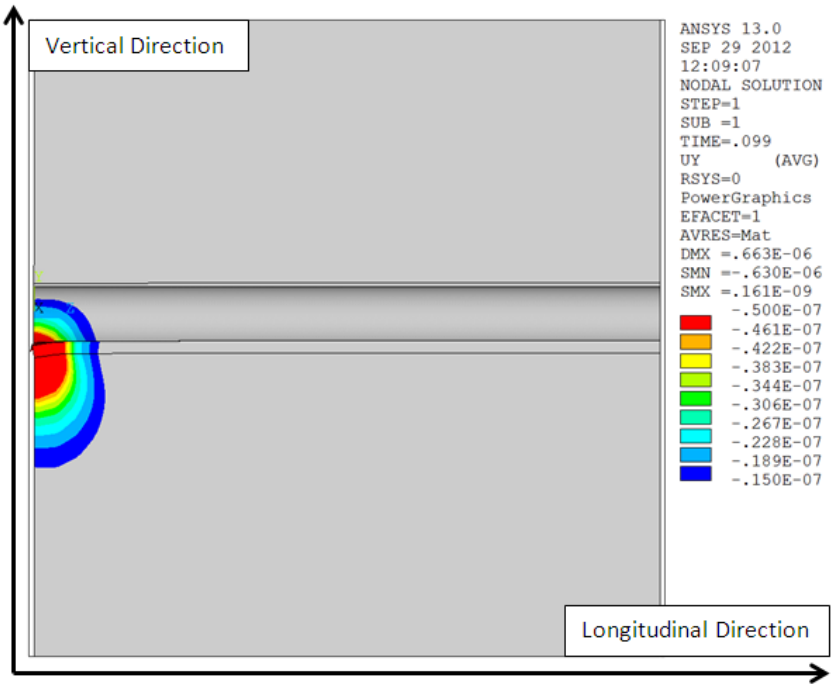


Figure 4.15 Vibration propagation in tunnel step 1

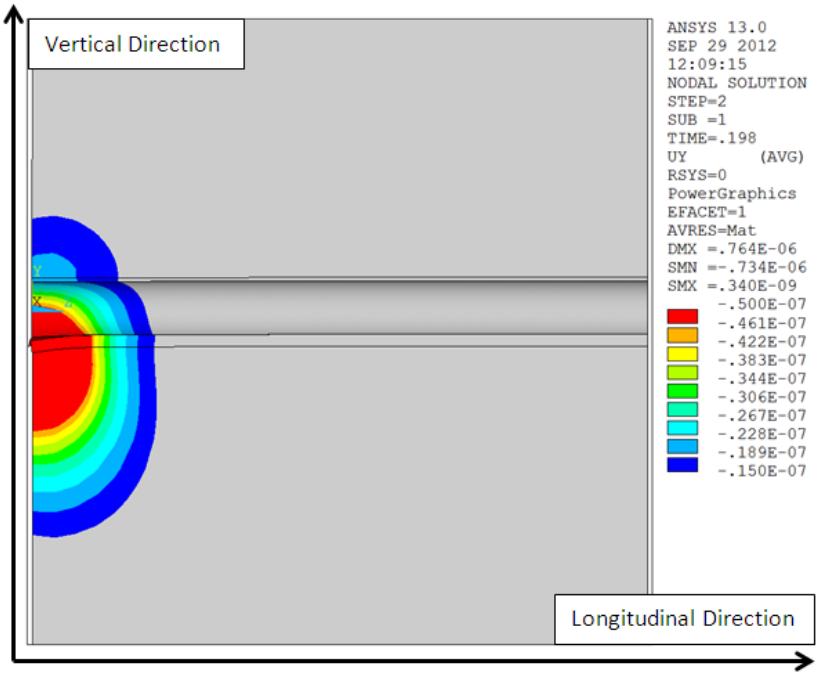


Figure 4.16 Vibration propagation in tunnel step 2

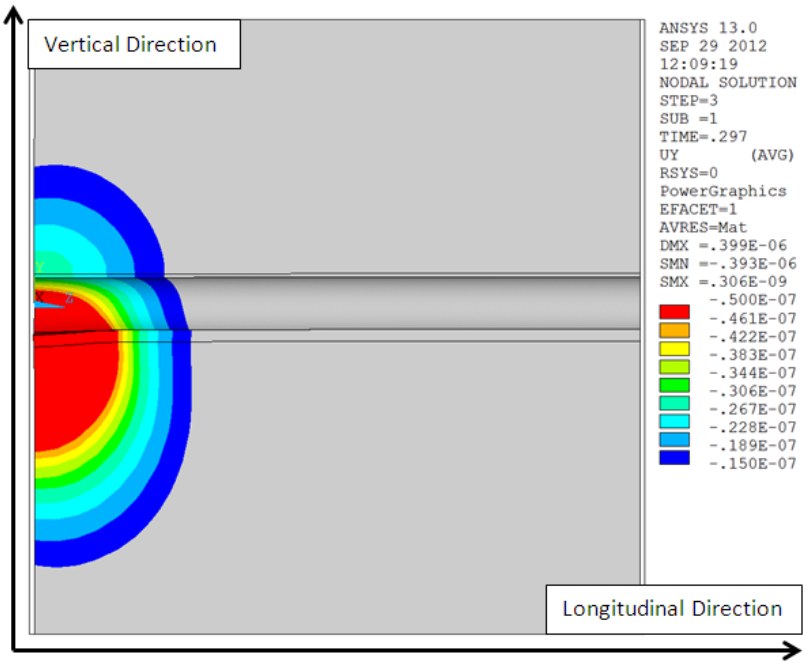


Figure 4.17 Vibration propagation in tunnel step 3

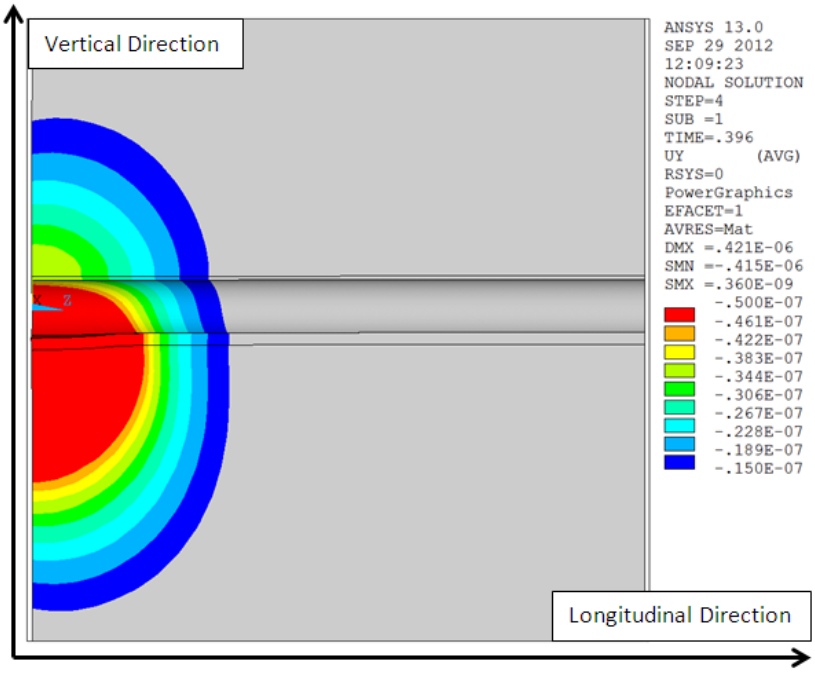


Figure 4.18 Vibration propagation in tunnel step 4

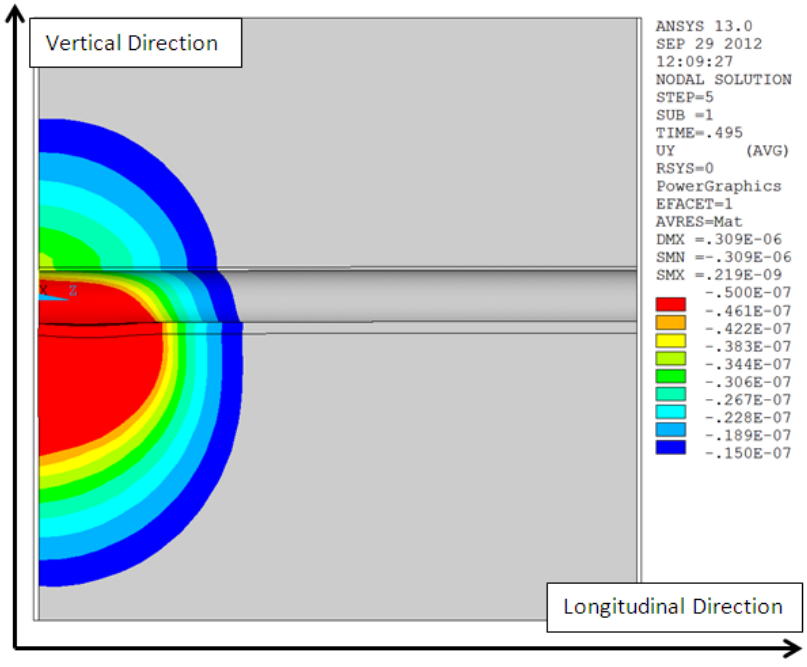


Figure 4.19 Vibration propagation in tunnel step 5

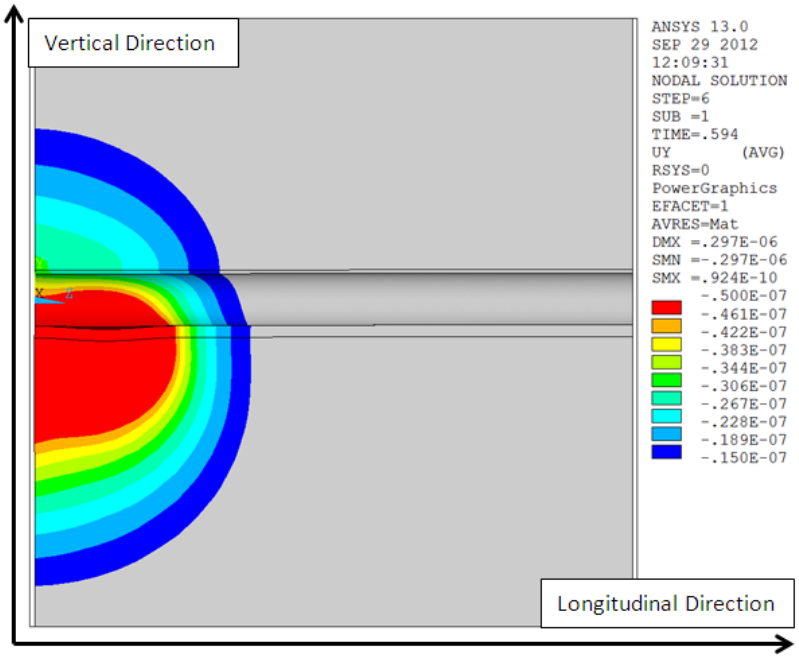


Figure 4.20 Vibration propagation in tunnel step 6

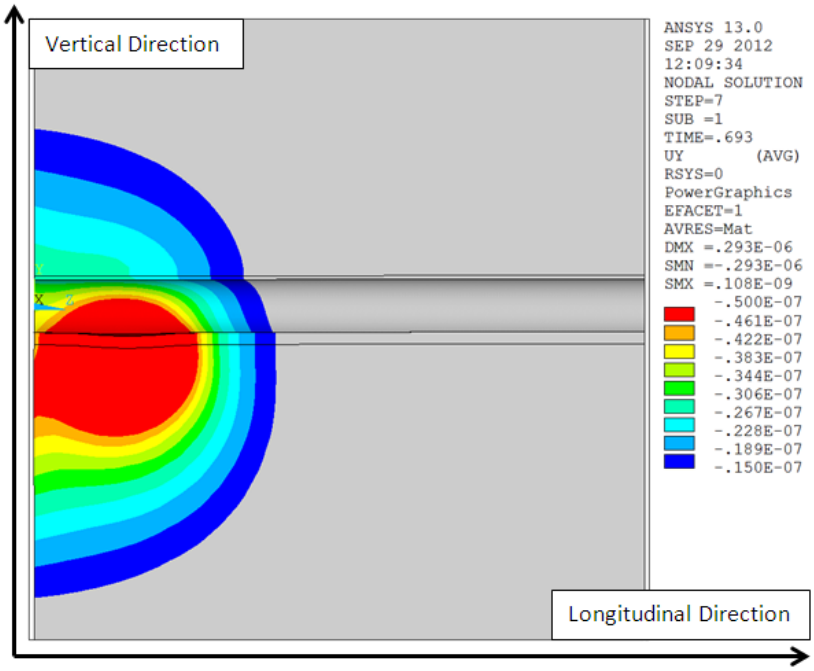


Figure 4.21 Vibration propagation in tunnel step 7

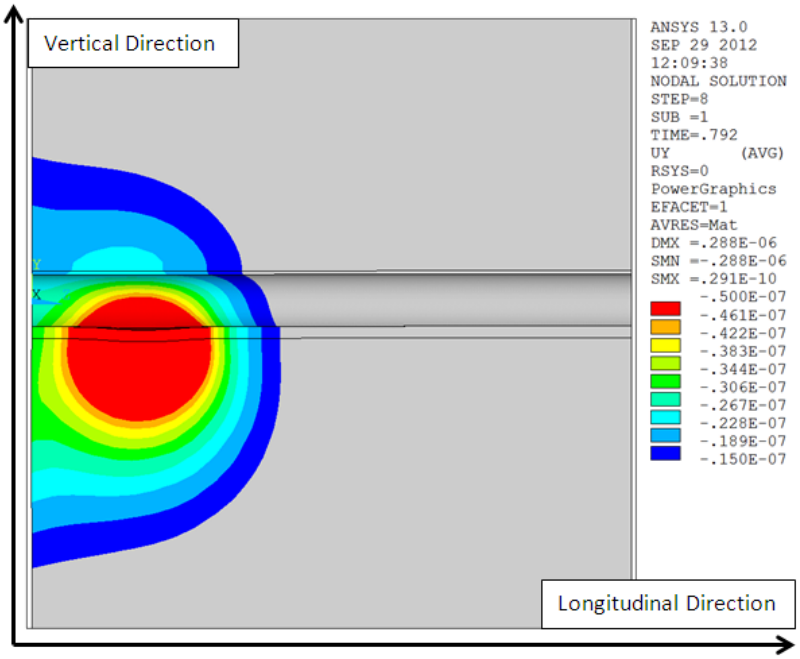


Figure 4.22 Vibration propagation in tunnel step 8

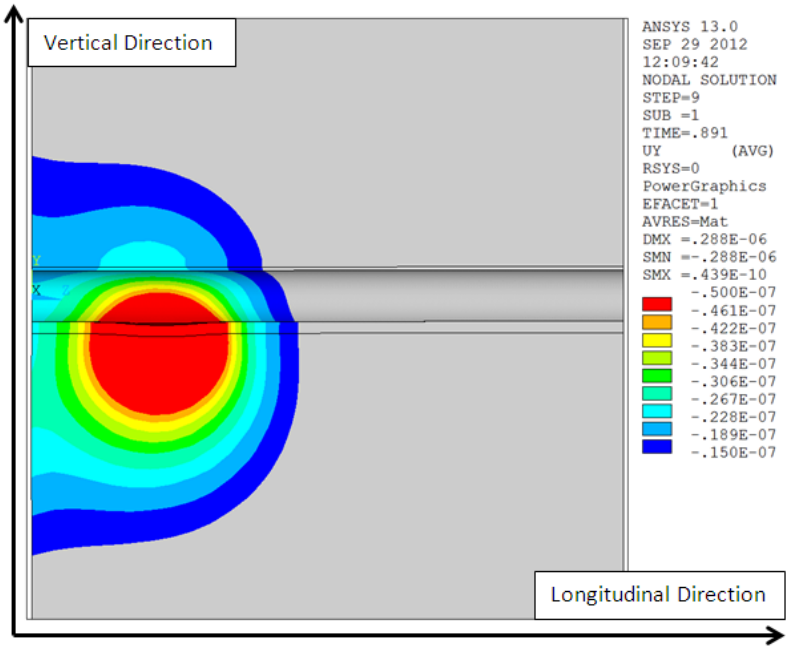


Figure 4.23 Vibration propagation in tunnel step 9

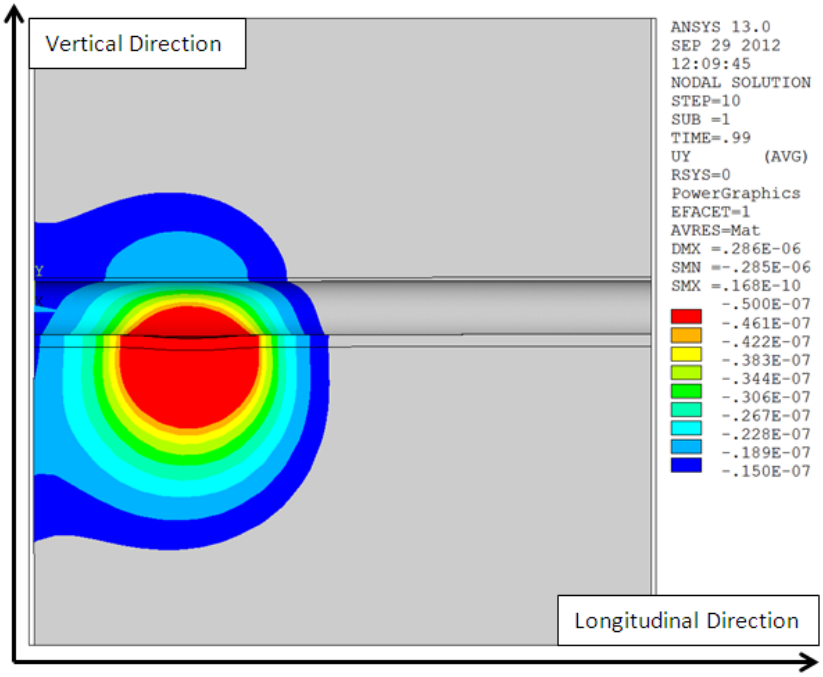


Figure 4.24 Vibration propagation in tunnel step 10

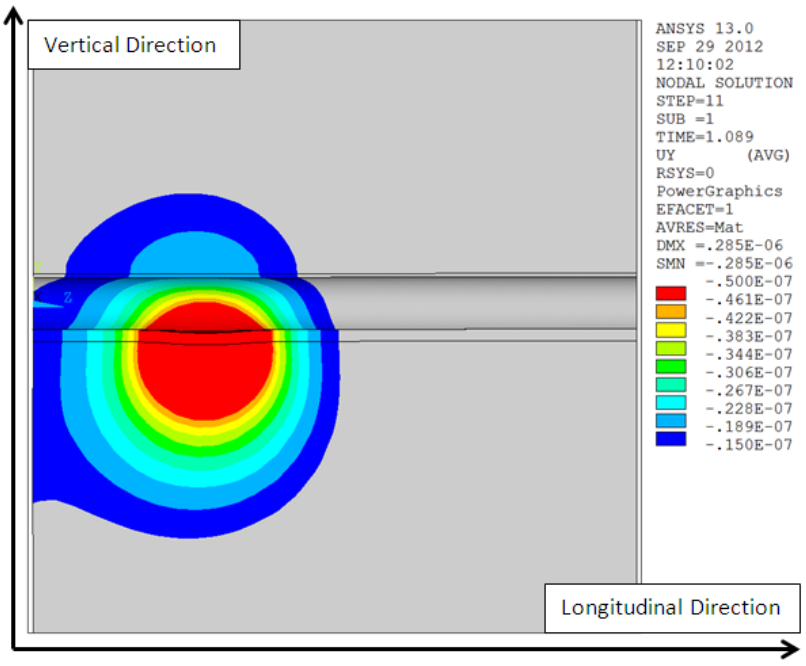


Figure 4.25 Vibration propagation in tunnel step 11

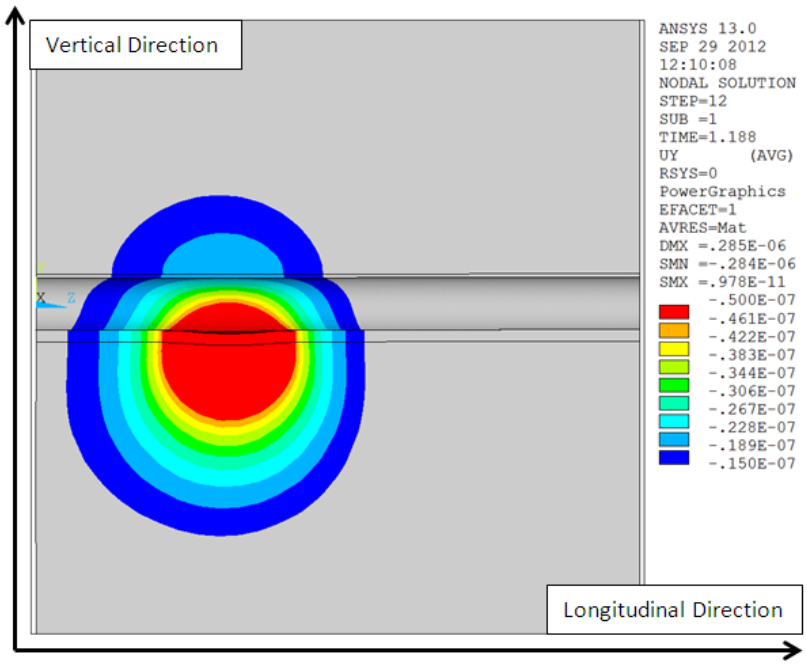


Figure 4.26 Vibration propagation in tunnel step 12

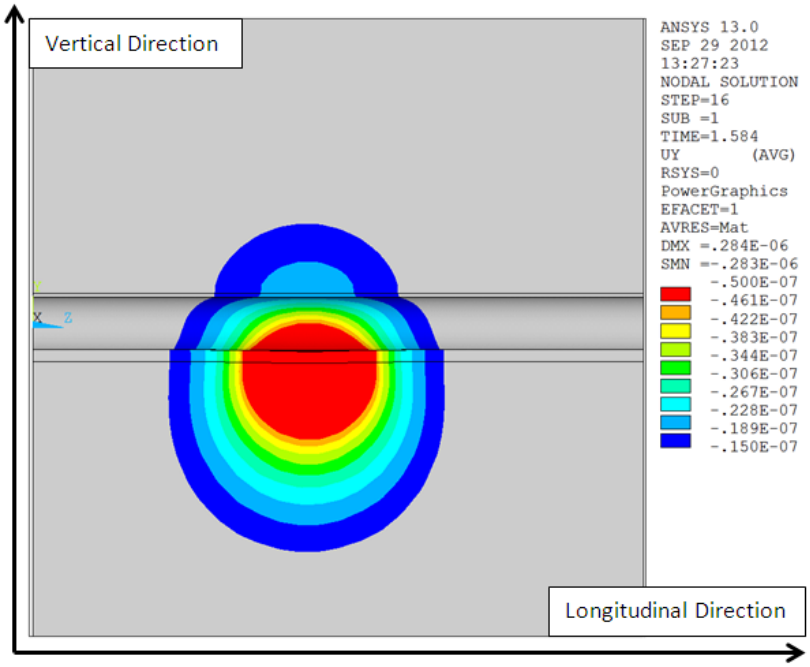


Figure 4.27 Vibration propagation in the middle of tunnel step 16

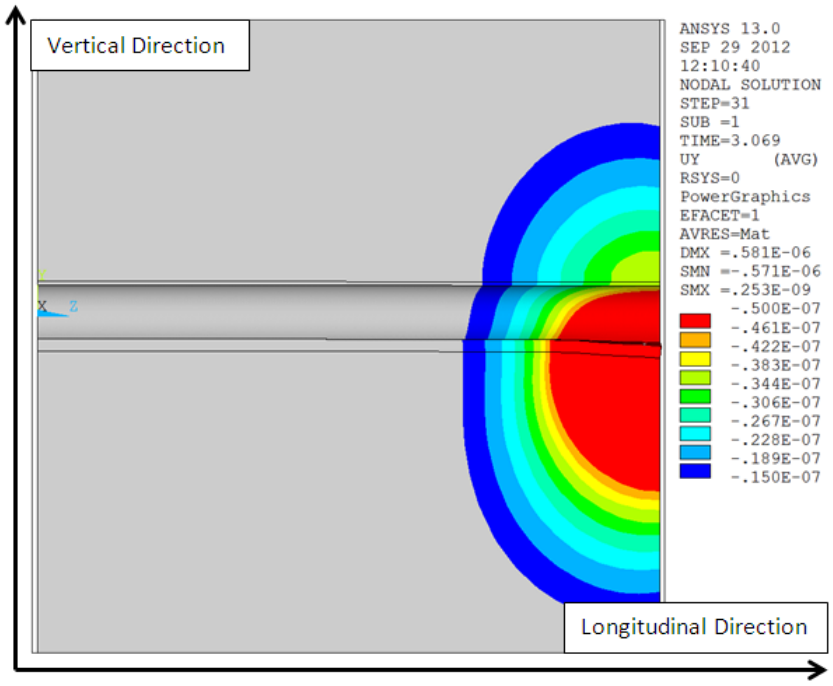


Figure 4.28 Vibration propagation at the end of tunnel step 31

# CHAPTER 5

## CONCLUSIONS

In this thesis ground-borne vibrations from underground railway systems are modeled by using commercial finite element software. The model is based on Forrest and Hunt's model [11]. The finite element model is kept as simple as possible and assumptions are made to simplify calculations without losing integrity with the real problem. The modeling is based on the track configuration of Kadıköy-Kartal Metro Line in the reference [52].

The three dimensional model consists of 245881 elements and 353910 nodes. The maximum element size is calculated according to the fact that model must be constructed on the principle that 6 elements are defined for each wavelength corresponding to the maximum frequency of interest, i.e., 80 Hz. The computational time with provided criteria above takes about 120 hours, i.e., 5 days, for one soil type on quadcore high performance computers. Transient analysis is possible with this modeling approach and results are obtained for both frequency and time domains.

In the study, parametric case studies are conducted to reveal the effects of soil type, railpad and train speed on vibration characteristics. Stiff and soft soil are investigated. It is observed approximately 3 order of magnitude difference occurs between stiff and soft soils. Vibration level

decreases while the radial distance in soil from the top of the rail increases for both soil types. The trend of the vibration level in frequency domain depends directly on the force excitation. The results in frequency domain show similar trend as the analytical results in the reference [52] which uses the same track configuration and the same model parameters.

Railpad 1 is provided from Kadıköy-Kartal Metro Line. Railpad 2 properties are obtained from reference [53] to design a case study. After performing an analysis with two different railpads, it is revealed that railpad properties affect the whole system characteristics. In the figures for frequency domain, there are two peaks for railpad 1 case and there is one peak for railpad 2. It is speculated that the second peak may be shifted out of the interested frequency range owing to the increased stiffness of the rail pad.

A final parametric study is conducted with train speeds. Mostly, train speed of 80 km/h, which is design speed of Kadıköy-Kartal Metro Line, is used in the analyses. The change in vibration behavior is obsevered when train speed is increased from 80 km/h to 100 km/h. It is realized that the amplitudes of the vibration velocity are approximately two times increased when speed increases.

Transient analysis results show that that softer soil produce higher vibration amplitudes than stiffer soil. However, vibration is damped faster, that is, in shorter distance in softer soil.

In the analyses, soil is modeled as a hollow thick cylinder and its exterior surface is fixed. The thickness of the soil is 50 meters which needs to be sufficiently high to damp the vibration energy in its entire thickness such that vibrational waves should not be reflected from boundary.

Therefore, an extra analysis is performed with infinite boundary conditions to validate the thickness of the soil. Vibrational waves propagate further in stiff soil; therefore, the stiffer soil, soil B is analysed in the frequency range of 1-80 Hz. The result of the infinite boundary condition case comes out to be very close to the fixed boundary case. Therefore, fixed boundary conditions can be readily applied with this soil thickness.

Another study is carried on the directional characteristics of the vibration whether it is upwards or downwards. It is revealed that in downward direction, vibration decreases faster due to the proximity of soil to the track. It is hypothesized that the energy in propagation of vibrational waves may be damped out by tunnel in upward direction.

Finally, the propagation of the vibration along the tunnel is shown step by step in order to understand the behavior of vibration while propagating in the tunnel. It is understood that vibration waves attenuate more in upward direction due to the tunnel acting like buffer zone.

Future works to improve this model can be devised. Non-linear effects associated with soil behavior can be taken into consideration in modeling and different track configurations can be applied to the model. On the finite element side, other element types can be tested, for example, rail can be modeled with another type of beam element, BEAM189. Different design parameters associated with the trackwork can be selected to assist in the design process. Experimental studies in the form of vibration measurements on Kadıköy-Kartal metro line needs to be designed to assess the accuracy and power of the analysis.

## REFERENCES


[1] R. J. Diehl, R. Nowack and G. Hölzl; Solutions for Acoustical Problems with Ballastless Track; Journal of Sound and Vibration 231(3) (2000) 899-906

[2] Typical Rail Section; http://www.foresthistory.org/ASPNET/Publications/region/3/lincoln/cultres4/sec3.htm; last visited on 21st of August 2012

[3] Johannes Jacobus Heunis; Material models for rail pads; MSc Thesis; Department of Mechanical and Mechatronic Engineering, University of Stellenbosch, Western Cape (2011)

[4] Huan Feng; 3D-models of Railway Track for Dynamic Analysis; M.Sc. Thesis; Department of Transport Science; Royal Institute of Technology, Stockholm (2011)

[5] M. Sarıgöl; Modeling of ground-borne vibration from underground railway systems, M.Sc. Thesis, Department of Mechanical Engineering, Middle East Technical University, Ankara (2007)

[6] Kurzweil L. G.; Ground-Borne Noise and Vibration from Underground Rail Systems; Journal of Sound and Vibration 66(3) (1979) 363-370

[7] D. Clouteau, M. Arnst, T.M. Al-Hussaini, G. Degrande; Freefield Vibrations Due To Dynamic Loading On A Tunnel Embedded In A Stratified Medium; Journal of Sound and Vibration 283 (2005)173–199

[8] Forrest J.A., Hunt H.E.M.; A Three-Dimensional Tunnel Model for Calculation of Train-Induced Ground Vibration; Journal of Sound and Vibration 294 (2006) 678-705

[9] Andreas Eitzenberger; Train-induced Vibrations in Tunnels – A Review; Technical Report; Department of Civil, Mining and Environmental Engineering; Luleå University of Technology, Luleå (2008)

[10] Remington. P.J., Kurtweil, L.G. and Tower. D.A.; Low-Frequency Noise And Vibrations From Trains. In: Transportation Noise Reference Book; Ed. Nelson. P.M. London: Butterworths (1987)

[11] J.A. Forrest, H.E.M Hunt; Ground Vibration Generated By Trains In Underground Tunnels; Journal of Sound and Vibration 294 (2006) 706-736

[12] Möller, B., Larsson, R., Bengtsson, P-E. and Moritz, L. (2000). Geodynamik i praktiken. Linköping: Swedish Geotechnical Institute

[13] Hall, L.; Simulations And Analyses Of Train-Induced Ground Vibrations In Finite Element Models; Soil Dynamics and Earthquake Engineering 23 (2003) 403–413

[14] Gardien W., Stuit H.G.; Modeling of Soil Vibrations from Railway Tunnels; Journal of Sound and Vibration 267 (2003) 605–619

[15] Hussein M.F.M., Hunt H.E.M.; A Power Flow Method For Evaluating Vibration From Underground Railways; Journal of Sound and Vibration 293 (2006) 667–679

[16] Karlström A., Boström R.; An Analytical Model for Train-Induced Ground Vibrations from Railways; Journal of Sound and Vibration 292 (2006) 221–241

[17] Sheng X., Jones C.J.C., Petyt M.; Ground Vibration Generated By A Harmonic Load Acting On A Railway Track; Journal of Sound and Vibration 225(1) (1999) 3-28

[18] Sheng X., Jones C.J.C., Petyt M.; Ground Vibration Generated By A Load Moving Along A Railway Track; Journal of Sound and Vibration 228(1) (1999) 129-156

[19] Takemiya H.; Simulation of Track–Ground Vibrations Due To A High-Speed Train: The Case of X-2000 at Ledsgard; Journal of Sound and Vibration 261 (2003) 503–526

[20] Chen Y.H., Huang Y.H., Shih C.T.; Response Of An Infinite Timoshenko Beam on a Viscoelastic Foundation to a Harmonic Moving Load, Journal of Sound and Vibration 241(5) (2001) 809-824

[21] M.H. Kargarnovin, D. Younesian, D.J. Thompson, C.J.C. Jones; Response Of Beams On Nonlinear Viscoelastic Foundations To Harmonic Moving Loads; Computers and Structures 83 (2005) 1865–1877

[22] Hou K., Kalousek J., Dong R.; A Dynamic Model for an Asymmetrical Vehicle/Track System; Journal of Sound and Vibration 267 (2003) 591–604

[23] Sun Y.Q., Dhanasekar M.; A Dynamic Model for the Vertical Interaction of the Rail Track and Wagon System; International Journal of Solids and Structures 39 (2002) 1337–1359

[24] Verichev S.N., Metrikine A.V.; Instability Of A Bogie Moving On A Flexibly Supported Timoshenko Beam; Journal of Sound and Vibration 253(3) (2002) 653-668

[25] Wu T.X., Thompson D.J.; A Double Timoshenko Beam Model for Vertical Vibration Analysis of Railway Track at High Frequencies; Journal of Sound and Vibration 224(2) (1999) 329-348

[26] Shuguang Zhang, Xinbiao Xiao, Zefeng Wen, Xuesong Jin; Effect Of Unsupported Sleepers On Wheel/Rail Normal Load; Soil Dynamics and Earthquake Engineering 28 (2008) 662–673

[27] Knothe K.L., Grassie S.L.; Modeling of Railway Track and Vehicle/Track Interaction at High Frequencies; Vehicle System Dynamics 22 (1993) 209-262

[28] P. Galvin, A.Romero, J.Dominguez; Vibrations Induced By HST Passage On Ballast And Non-Ballast Tracks; Soil Dynamics and Earthquake Engineering 30 (2010) 862–873

[29] Zhai, W.M., Wang, K.Y. and Lin, J.H.; Modeling and Experiment of Railway Ballast Vibrations; Journal of Sound and Vibration 270 (2004) 673 – 683

[30] Lombaert, G., Degrande, G., Vanhauwere, B., Vandeborght, B. and François, S.; The Control Of Ground-Borne Vibrations From Railway Traffic By Means Of Continuous Floating Slabs; Journal of Sound and Vibration 297 (2006) 946 – 961

[31] L. Andersen, C.J.C. Jones; Coupled Boundary and Finite Element Analysis of Vibration from Railway Tunnels - A Comparison of Two - And Three-Dimensional Models; Journal of Sound and Vibration 293 (2006) 611–625

[32] A. M. Remennikov, S. Kaewunruen; Determination Of Dynamic Properties Of Rail Pads Using An Instrumented Hammer Impact Technique; Acoustics Australia 33(2) (2005) 63-67

[33] Gutowski T.G., Dym C.L.; Propagation of Ground Vibration: A Review; Journal of Sound and Vibration 49(2) (1976) 179-193

[34] B. Picoux, D. Le Houédec; Diagnosis And Prediction Of Vibration From Railway Trains; Soil Dynamics and Earthquake Engineering 25 (2005) 905–921

[35] D. V. Jones, D. Le Houedec, A. T. Peplow and M. Petyt; Ground Vibration In The Vicinity Of A Moving Harmonic Rectangular Load On A Half-Space; ELII: J. Mech., A/Solids, 17 no I. (1998) 153-l 66

[36] H.-H. Hung, Y. and B. Yang; Elastic Waves In Viscoelastic Half Space Generated By Various Vehicle Loads; Soil Dynamics and Earthquake Engineering 21 (2001) 1-17

[37] O. Chupin, A. Chabot, J.-M. Piau; D. Duhamel; Influence Of Sliding Interfaces On The Response Of A Layered Viscoelastic Medium Under A Moving Load; International Journal of Solids and Structures 47 (2010) 3435–3446

[38] Lefeuve-Mesgouez G., Peplow A.T., Le Houédec D.; Ground Vibration In The Vicinity Of A High-Speed Moving Harmonic Strip Load; Journal of Sound and Vibration 231(5) (2000) 1289–1309

[39] Popp K., Kruse H., Kaiser I., Vehicle-Track Dynamics in the Mid-Frequency Range, Vehicle System Dynamics 31 (1999) 423-464

[40] Egidio Di Gialleonardo, Francesco Braghin, Stefano Bruni; The Influence of Track Modeling Options on the Simulation of Rail Vehicle Dynamics; Journal of Sound and Vibration 331 (2012) 4246–4258

[41] George T. Michaltsos, Ioannis G. Raftoyiannis; The Influence Of A Train's Critical Speed And Rail Discontinuity On The Dynamic Behavior Of Single-Span Steel Bridges; Engineering Structures 32 (2010) 570-579

[42] Jens C.O. Nielsen; High-Frequency Vertical Wheel–Rail Contact Forces—Validation Of A Prediction Model By Field Testing; Wear 265 (2008) 1465–1471

[43] X. Sheng, C.J.C. Jones and D.J. Thompson; A Theoretical Model For Ground Vibration From Trains Generated By Vertical Track Irregularities; Journal of Sound and Vibration 272 (2004) 937–965

[44] Sinan Al Suhairy; Prediction Of Ground Vibration From Railways; M.Sc. Thesis; SP Swedish National Testing and Research Institute; SP Report 2000:25; Boras (2000)

[45] Lei X., Noda N.A.; Analyses of Dynamic Response of Vehicle and Track Coupling System with Random Irregularity of Track Vertical Profile; Journal of Sound and Vibration 258(1) (2002) 147–165

[46] Grassie S.L., Gregory R.W., Harrison D., Johnson K.L.; The Dynamic Response of Railway Track to High Frequency Vertical Excitation; Journal of Mechanical Engineering Science 24 (1982) 77-90

[47] Wu T.X., Thompson D.J.; Theoretical Investigation of Wheel/Rail Non-Linear Interaction Due To Roughness Excitation; Vehicle System Dynamics 34 (2000) 261–282

[48] J Wang, X Jin, and Y Cao; High-Speed Maglev Train-Guideway-Tunnel-Soil Modeling Of Ground Vibration; Journal of Rail and Rapid Transit; Proc. IMechE Vol. 000 (2011) Part F

[49] Lars Hall; Simulations And Analyses Of Train-Induced Ground Vibrations In Finite Element Models; Soil Dynamics and Earthquake Engineering 23 (2003) 403–413

[50] F. Frederich, Die Gleislage –aus fahrzeugtechnischer Sicht [Effect of track geometry on vehicle performance], Zeitschrift für Eisenbahnwesen und Vekehrstechnik– Glasers Annalen 108 (1894) 355-362.

[51] J. Bitzenbauer and J. Dinkel; Dynamic Interaction between A Moving Vehicle and an Infinite Structure Excited By Irregularities – Fourier Transform Solutions; Archive of Applied Mechanics 72 (2002) 199-211

[52] S. Alan, M. Çalışkan; Experience with Random Process Theory on Prediction of Ground Borne Vibration from Underground Metro Systems; ICSV 18, Brazil (2011)

[53] Johanna Lilja, Thomas J.S. Abrahamsson, Jens C.O. Nielsen; Experimental Investigation of Stochastic Boundary Conditions - Planning A Railway Sleeper Test; Conference: IMAC-XXIV: Conference & Exposition on Structural Dynamics (2006)

[54] Advanced Analysis Techniques Guide, Documentation for ANSYS, ANSYS Inc., (2009)

[55] MATLAB R2008a User Manual, The MathWorks, Inc., (2008)